Published in final edited form as:

J Inorg Biochem. 2017 December ; 177: 171–182. doi:10.1016/j.jinorgbio.2017.09.018.

Covalent Attachment of the Heme to *Synechococcus* Hemoglobin Alters its Reactivity Toward Nitric Oxide

Matthew R. Preimesberger, **Eric A. Johnson**, **Dillon B. Nye**, and **Juliette T.J. Lecomte**

T.C. Jenkins Department of Biophysics, Johns Hopkins University, Baltimore, MD 21218, USA.

Abstract

The cyanobacterium *Synechococcus* sp. PCC 7002 produces a monomeric hemoglobin (GlbN) implicated in the detoxification of reactive nitrogen and oxygen species. GlbN contains a *b* heme, which can be modified under certain reducing conditions. The modified protein (GlbN-A) has one heme–histidine C–N linkage similar to the C–S linkage of cytochrome *c*. No clear functional role has been assigned to this modification. Here, optical absorbance and NMR spectroscopies were used to compare the reactivity of GlbN and GlbN-A toward nitric oxide (NO). Both forms of the protein are capable of NO dioxygenase activity and both undergo heme bleaching after multiple NO challenges. GlbN and GlbN-A bind NO in the ferric state and form diamagnetic complexes (Fe^{III}–NO) that resist reductive nitrosylation to the paramagnetic Fe^{II}–NO forms. Dithionite reduction of Fe^{III}–NO GlbN and GlbN-A, however, resulted in distinct outcomes. Whereas GlbN-A rapidly formed the expected Fe^{II}–NO complex, NO binding to Fe^{II} GlbN caused immediate heme loss and, remarkably, was followed by slow heme rebinding and HNO (nitrosyl hydride) production. Additionally, combining Fe^{III} GlbN, ^{15}N-labeled nitrite, and excess dithionite resulted in the formation of Fe^{II}–H^{15}NO GlbN. Dithionite-mediated HNO production was also observed for the related GlbN from *Synechocystis* sp. PCC 6803. Although ferrous GlbN-A appeared capable of trapping preformed HNO, the histidine–heme post-translational modification extinguished the NO reduction chemistry associated with GlbN. Overall, the results suggest a role for the covalent modification in Fe^{II} GlbNs: protection from NO-mediated heme loss and prevention of HNO formation.

Keywords

Truncated hemoglobin; nitric oxide dioxygenase; nitric oxide reductase; nitrite reductase; nitrosyl hydride; nitroxyl

1. Introduction

Nitric oxide (NO) is a reactive molecule and a potential actor in a variety of cellular processes [1, 2]. As such, its concentration must be carefully regulated under a wide range of physiologic conditions. In plants and many microorganisms, NO can be produced reductively as an intermediate along the nitrate assimilation or denitrification pathways [3, 4]. Other reductive routes as well as oxidative processes [5] can destroy NO. Heme proteins

Tel: (410) 516-7019. Fax: (410) 516-4118. lecomte_jtj@jhu.edu.

such as hemoglobins (Hbs) are a priori able to switch between source and sink activities and therefore warrant investigation as particularly responsive regulators of free NO concentration. High levels of reactive oxygen and nitrogen species, along with a connection between NO metabolism and release of the potent green-house gas nitrous oxide (N_2O), focus attention on the hemoglobins of abundant photosynthetic unicellular organisms.

The model cyanobacterium *Synechococcus* sp. PCC 7002 (*Synechococcus* hereafter) contains a gene (*glbN*) encoding a hemoglobin (GlbN) of the group 1 truncated lineage (TrHb1) [6]. As purified after recombinant expression in *Escherichia coli*, apoGlbN binds a *b* heme (iron-protoporphyrin IX) with two axial histidines, His46 and His70, in both the ferric (Fe^{III}) (Figure S1A) and ferrous (Fe^{II}) heme oxidation states [7]. In the presence of exogenous ligands such as CO and CN^-, His46 (the “distal” heme ligand) can be reversibly displaced from the ferrous or ferric iron (respectively) whereas His70 (the “proximal” heme ligand) remains coordinated [6, 8] (Figure S1A).

Along with ferrous *Synechocystis* sp. PCC 6803 GlbN (*Synechocystis* GlbN hereafter), ferrous *Synechococcus* GlbN is extraordinary among hemoglobins (Hbs) for undergoing a spontaneous and irreversible posttranslational modification (PTM) with the heme group. Specifically, the GlbN PTM consists in the saturation of the 2-vinyl substituent, covalently attaching the heme to His117 Nε2 [9] (Figure S1B). The PTM is facile in that it can be engineered to occur at the 4-vinyl (Leu79His/His117Ala variant of *Synechocystis* GlbN and Leu75His variant of *Chlamydomonas eugametos* LI637 CtrHb) and even both the 2- and 4-vinyls (Leu79His variant of *Synechocystis* GlbN) [10, 11]. Many cyanobacterial TrHb1s have strong sequence identity around a highly conserved His117 and are suspected to undergo the PTM as well. The structural [8] and dynamic [7] properties of wild-type (WT) *Synechococcus* GlbN and GlbN with PTM (hereafter GlbN-A) are similar. GlbN-A, incapable of heme loss, has increased thermodynamic stability [12], but other consequences of histidine-heme cross-linking have not been investigated.

Mechanistic studies support that the ferrous heme PTM occurs via an electrophilic addition [13, 14]. Starting with apoGlbN reconstituted with ferric heme, the reaction is inhibited if reduction is performed in the presence of CO, presumably because this small ligand binds to ferrous GlbN rapidly and withdraws electron density from the porphyrin π-system through back-bonding [14]. Dioxygen is expected to have a deactivating effect as well through its propensity for superoxide formation ($Fe^{III}–O_2^-$) when bound to ferrous heme [15].

The biological function of GlbN and its modified form has not yet been ascertained. Several studies of the transcriptome of *Synechococcus* cells have detected constitutive expression of *glbN* [16–18]. When overexpressed under microoxic conditions, the protein contains covalently attached heme whereas oxic conditions appear to favor unmodified GlbN [16]. Thus, both GlbN and GlbN-A are candidates for physiological relevance, and the PTM may act as a sensor for cellular redox and oxygen status. Elevated levels of reactive oxygen/nitrogen species (ROS/RNS) are detected in a *Synechococcus glbN* knock-out strain under both aerobic and microoxic growth on nitrate [16]. Although stress from oxygen, temperature, salt, and various medium components did not result in substantial changes to expression levels of *glbN*, it is of note that expression under these conditions roughly

matched that of other transcripts for genes *(sodB*, *katG*, *msrA*, *msrB*, etc.) encoding proteins known to mitigate ROS/RNS damage [17]. These in vivo observations suggest that GlbN and GlbN-A participate in nitrogen-oxygen chemistry and implicate the heme crosslink in modulating the response.

We have shown previously that *ΔglbN Synechococcus* cells are more susceptible to nitric oxide (NO) challenge than wild-type cells and that they accumulate higher levels of ROS/RNS [16]. Dedicated NO synthases have not been identified in *Synechococcus*, but the reduction of nitrate to ammonia likely releases NO adventitiously via enzymes such as nitrate reductase (NarB) [19] as has been observed in plants [20]. In the absence of O_2, ferrous GlbNs are themselves another potential source of NO via their nitrite reductase activity [21]. Released NO can then undergo diffusion-limited combination with superoxide to form the powerful oxidant peroxynitrite ($O{=}NOO^-$), its conjugate acid, and various nitrogen oxides [22–25]. These RNS, like ROS, attack cellular components and require active management. Of particular importance in cyanobacteria is the reaction of NO and NO-derived species with heme proteins, iron-sulfur clusters [26], and free thiols [27, 28], which would interfere with photosynthesis and respiration, among other cellular processes.

In this work, we inspect the NO chemistries of GlbN and address differences in the in vitro reactivity of GlbN and GlbN-A. We show that GlbN and GlbN-A can oxidize NO through nitric oxide dioxygenation, but that both proteins undergo heme bleaching during such activity. We also provide evidence that GlbN, but not GlbN-A, has the remarkable capability of reducing NO to HNO at neutral pH using the common reductant dithionite as the electron source. The differential reactivity allowed us to propose a protective role for the histidine–heme PTM.

2. Materials and Methods

2.1 Protein preparation

Wild-type (WT) *Synechococcus* GlbN, H117A *Synechococcus* GlbN, WT *Synechocystis* GlbN, and WT *Chlamydomonas reinhardtii* THB1 were produced in *Escherichia coli* without affinity tag as described previously [6, 29, 30]. All globins are prepared in the ferric state by reconstitution of the purified apoprotein with hemin. Horse skeletal myoglobin was purchased from Sigma. Its apoprotein was prepared by the method of Teale [31].

The (heme-free) diaphorase domain of the *C. reinhardtii* nitrate reductase (NR) was produced through heterologous expression in *E. coli*. The protein consists of the C-terminal end of the native NR [32] beginning at residue K509. The corresponding amino acid sequence for this portion of the protein was codon-optimized for bacterial expression and synthesized as double stranded DNA (IDT, Coralville, IA, USA). The synthesized gene was fused at its N-terminus to a sequence encoding a polyhistidine tag and PreScission protease cleavage site within a pET28 expression plasmid. The protein was expressed at 27 °C for 20 h using LB medium supplemented with 50 μg/mL kanamycin and 0.1 mg/mL riboflavin to boost flavin adenine dinucleotide (FAD) incorporation. Under these conditions, expressed soluble protein incorporated the FAD cofactor and no heme. The soluble protein was bound to a Ni-NTA column and eluted with 100 mM imidazole. The protein was dialyzed

extensively with 20 mM Tris-HCl pH 8.0, 20 mM NaCl to remove imidazole. 0.1 mg/mL PreScission protease (GE Healthcare) was added prior to dialysis. The cleaved N-terminal tag was eliminated by a subsequent pass through the Ni-NTA column, which also removed the polyhistidine-tagged protease. The concentration of the resulting active protein solution was determined using the free FAD concentration following cofactor release with 0.5% SDS and using an extinction coefficient $\varepsilon_{450} = 11.3\ mM^{-1}\ cm^{-1}$ [33]. The protein was lyophilized and stored at −80 °C until used.

2.2 Preparation of GlbN-A from GlbN

To prepare GlbN-A from GlbN, a concentrated solution of ferric GlbN (typically 1–2 mM) in 50–250 mM Na/K-phosphate pH 7.0–7.2 was reduced with a 5-fold molar excess of freshly prepared sodium dithionite (DT, Alfa-Aesar). At this pH, the conversion of ferrous GlbN to ferrous GlbN-A is completed in less than 10 s. For storage, the protein was oxidized to the ferric state by addition of excess potassium ferricyanide and purified by passage through a G-25 desalting column.

2.3 Glucose oxidase/D-(+)-glucose/catalase O_2 scavenging system

To generate in vitro microoxic conditions, we used the glucose oxidase/D-(+)-glucose/catalase (GODCAT) O_2 elimination system [34]. For optical absorbance experiments, individual components included (final concentrations): 40 μg/mL bovine catalase (Sigma), 100–200 μg/mL *Aspergillus niger* glucose oxidase (Sigma), and 0.04% m/v D-glucose. For NMR experiments, the catalase and glucose oxidase concentrations were doubled. At these concentrations the GODCAT system depleted most dissolved O_2 present in a small solution volume in under 5 min as determined using an oxygen electrode.

2.4 Ferredoxin/$NADP^+$ and nitrate reductase diaphorase reduction systems

When reduction under oxic conditions was required, two alternative enzymatic systems were used. The first was a ferredoxin-based system [35], which contains glucose 6-phosphate (G6P) as the initial source of electrons, G6P dehydrogenase (G6P DH) to generate NADPH from G6P and $NADP^+$, and ferredoxin-$NADP^+$ reductase (FNR) to reduce spinach ferredoxin (Fd). Typical optical absorbance experiments included the following components (all from Sigma, final concentrations): 0.1 % m/v G6P, 0.01–0.2 mM $NADP^+$, ~20 U *Leuconostoc mesenteroides* G6P DH, ~0.1 U spinach FNR, 100–500 μg/mL Fd, and 40 μg/mL bovine catalase to eliminate H_2O_2. Order-of-addition control experiments indicated that Fd was the active reductant for GlbNs. In variations of this protocol, some experiments were conducted by omitting the $NADP^+$/NADPH recycling system (G6P and G6P DH) and using NADPH (Sigma) instead of $NADP^+$. Such optical absorbance experiments included the following components: 25 mU spinach FNR, 0.5 μM Fd, 40 μg/mL catalase, 300 μM NADPH. NADPH alone failed to reduce Fe^{III} GlbN and GlbN-A. The second reduction system was composed of the heme-free diaphorase domain of *C. reinhardtii* NR and NADPH as the source of electrons, to circumvent possible long-term damage caused by NO to the Fd/FNR system. Optical experiments included 2 μM NR diaphorase and 300 μM NADPH.

2.5 Optical absorbance spectrophotometry

Absorbance data were acquired at room temperature on a Cary50 UV-vis spectrophotometer. Protein concentration was evaluated with the following coefficients: H117A and WT *Synechococcus* Fe^{III} GlbNs [6], ε_{411} = 96 mM^{-1} cm^{-1}; WT Fe^{III} GlbN-A, ε_{409} = 87 mM^{-1} cm^{-1}. Spectra were typically collected over 700–250 nm, with 0.5 s averaging time, and 1 nm step size. For kinetic measurements, this window was narrowed to the desired region and acquisition parameters were 0.1 s averaging time with 1 nm step size. Manual mixing dead times were ~15 s. Unless otherwise noted, optical spectra were collected every 0.5 min for 20 min, and then every 5 min for 2 h.

2.6 NO binding to Fe^{III} GlbNs monitored by optical absorbance

Stock solutions of the NO donors dipropylenetriamine-NONOate (DPTA-NONOate, Cayman Chemical) or methylamine hexamethylene methylamine-NONOate (MAHMA-NONOate, Cayman Chemical) were prepared in 0.1 M NaOH. The concentration was evaluated after dilution in H_2O using published extinction coefficients (DPTA-NONOate, ε_{252} = 7.9 mM^{-1} cm^{-1} [36]; MAHMA-NONOate, ε_{250} = 7.25 mM^{-1} cm^{-1} [37]). At pH 13, the NONOates were stable for days to weeks and degradation could be assessed by a decrease in the 250 nm absorbance band. At pH 7, the NONOates degrade by an apparent single exponential process (DPTA-NONOate, $t_{1/2}$ ~ 3–4 h, MAHMA-NONOate $t_{1/2}$ ~ 3–4 min) to produce two molecules of NO per one molecule donor. In order to produce Fe^{III}–NO forms for optical absorbance spectroscopy, Fe^{III} GlbN and GlbN-A (4–10 μM) samples were treated with 0.8–1 mM NONOate.

2.7 NO dioxygenase (NOD) assay

Fe^{III} GlbN or GlbN-A (20 μM, 50 mM Tris, pH 7.0–7.2) was incubated in O_2–saturated buffer (O_2, Airgas) and in the presence of a Fd reductase system to produce oxy (Fe^{II}–O_2) complexes. Conversion was followed optically and, when completed, MAHMA-NONOate was added to the specified concentration (typically 1.5-fold molar excess NO on a heme basis) to generate NO and initiate NOD activity. After oxidation, GlbN (or GlbN-A) was re-reduced by the enzyme system and returned to the Fe^{II}–O_2 form. For multiple NO addition experiments, MAHMA-NONOate was introduced after full recovery to the Fe^{II}–O_2 form. WT *C. reinhardtii* THB1 was treated similarly.

2.8 Reduction of Fe^{III}–NO GlbNs monitored by optical absorbance

Fe^{III} WT and H117A GlbNs were treated with DPTA- or MAHMA-NONOate to produce the Fe^{III}–NO (4–10 μM, pH 7.0–7.2) form. The Fe^{III}–NO GlbN(-A) was then treated with either 2 mM freshly prepared DT or the NR diaphorase reduction system (after incubation with GODCAT) to initiate reduction. As a test for heme loss upon Fe^{II}–NO formation, an ~ 8-fold molar excess (40–80 μM) of horse skeletal apomyoglobin was incubated with GlbN(-A) prior to the DT reduction step (~15 s). Under these conditions, heme dissociation from GlbN and capture by apomyoglobin (forming apoGlbN and Fe^{II}–NO myoglobin) can be monitored owing to the different visible spectra of GlbN and myoglobin nitrosyl complexes [38].

2.9 NMR spectroscopy of nitrosyl-GlbNs

NMR data were acquired on Bruker Avance or Avance-II NMR spectrometers operating at 600 MHz, each equipped with a cryoprobe. An unlabeled ~1.1 mM Fe^{III} GlbN sample (100 mM Na/K phosphate, pH 7.1, GODCAT, 298 K) was treated with four-fold excess MAHMA-NONOate to generate the Fe^{III}–NO state. A mixture of Fe^{III} and Fe^{III}–NO forms was produced and remained relatively stable for ~6 h. Water presaturation ^{1}H 1-D, ^{1}H-^{1}H NOESY (τ_{mix} = 80 ms), DQF-COSY, and TOCSY (τ_{mix} = 45 ms) spectra were recorded on the resulting sample in order to assign heme resonances. Because the Fe^{III}–NO form decayed in less than 12 h, only a preliminary analysis could be achieved. Similarly, an ^{15}N-labeled ~1.4 mM Fe^{III} GlbN-A (250 mM phosphate buffer, pH 7.1, GODCAT, 298 K) sample was treated with 5-fold molar excess MAHMA-NONOate to produce a mixture of Fe^{III} and Fe^{III}–NO GlbN-A. As above, water-presaturation ^{1}H 1-D, flip-back WATERGATE ^{1}H-^{1}H NOESY, and water-presaturation ^{1}H-^{1}H TOCSY spectra were acquired with ^{15}N-decoupling and used to assign heme resonances. ^{1}H-^{15}N HSQC spectra were recorded on a separate ^{15}N-labeled Fe^{III}–NO GlbN-A sample (800 μM protein, 5 mM DPTA-NONOate, 250 mM phosphate buffer, pH 7.1, 298 K). After data acquisition, the diamagnetic Fe^{III}–NO GlbN-A sample was treated with 8 mM DT, under argon (Airgas) atmosphere, and flip-back WATERGATE ^{1}H-^{15}N HSQC spectra were recorded on Fe^{II}–NO GlbN-A.

To generate the nitrosyl hydride complexes (Fe^{II}–HNO GlbN), two separate procedures were applied. 1) As above for the optical absorbance experiments, Fe^{III} GlbN was treated with MAHMA-NONOate to produce Fe^{III}–NO GlbN and subsequently reduced with excess DT. 2) Fe^{III} GlbN (or H117A GlbN) was incubated in the presence of nitrite or ^{15}N-labeled nitrite (NO_2^- or $^{15}NO_2^-$) and reduced with excess DT. Here, the nitrite reductase activity of GlbN was exploited to generate NO (or ^{15}NO) in situ. Procedures 1) and 2) both resulted in a mixture containing the same diamagnetic Fe^{II}–HNO (or Fe^{II}–$H^{15}NO$) form, which persisted for several hours. Water-presaturation^{1}H 1-D, NOESY, DQF-COSY, and flip-back WATERGATE ^{1}H-^{15}N HSQC spectra were used for heme and HNO assignments. To test for HNO formation in the absence of DT, ^{15}N-labeled H117A GlbN (~850 μM protein, 100 mM K/Na phosphate buffer, pH 7.1) was combined with $^{15}NO_2$ and the reduction system (5 μM heme-free NR diaphorase domain, 10 mM NADPH). ^{1}H 1-D and ^{1}H-^{15}N HSQC were then collected for several hours. Under those conditions, no ^{1}H-^{15}NO signal was detected.

2.10 NMR data processing and analysis

NMR data were processed using Topspin 1.3, Topspin 2.1, or NMRpipe [39]. Spectra were analyzed using Sparky 3 [40]. ^{1}H chemical shifts were referenced with respect to water (^{1}H = 4.76 ppm, 298 K). ^{15}N chemical shifts were referenced against liquid ammonia indirectly using the Ξ ratio [41].

2.11 Nomenclature used for GlbN nitrosyl complexes

In the text, Fe^{III}–NO or Fe^{II}–NO^+ refers to a $\{FeNO\}^6$ complex in Enemark-Feltham notation [42]. Fe^{II}–NO refers to a $\{FeNO\}^7$ complex and Fe^{II}–HNO or Fe^{II}–NO^- denotes a $\{FeNO\}^8$ complex.

3. Results

3.1 Ligand binding and electron transfer in bis–histidine GlbNs

Before inspecting GlbN reactions with NO, it is useful to present some common features related to heme hexacoordination. Most processes will require decoordination of the distal histidine to allow for exogenous ligand binding to iron (Equation 1a) and many will involve the loss or the gain of one electron, in conjunction with electron transfer (ET) from or to a redox partner. Two possible ET paths are illustrated with ferric state reduction (Equations 1b and 1c).

$$\text{His70} - \text{Fe}^{\text{II}} - \text{His46} \leftrightarrows \text{His70} - \text{Fe}^{\text{II}} + \text{His46} \quad (1a)$$

$$\text{His70} - \text{Fe}^{\text{III}} + e^{-} \rightarrow \text{His70} - \text{Fe}^{\text{II}} \quad (1b)$$

$$\text{His70} - \text{Fe}^{\text{III}} - \text{His46} + e^{-} \rightarrow \text{His70} - \text{Fe}^{\text{II}} - \text{His46} \quad (1c)$$

Under normal conditions of pH, temperature, and pressure, Equilibrium 1a favors strongly the hexacoordinated state through rapid k_{on} and slow k_{off} for His46 (k_{on}/k_{off} = K estimated to be ~ 300 for His46 in *Synechocystis* GlbN-A [43]). It is expected that reaction (1c), which uses the *bis*–histidine state, outcompetes reaction (1b) if distal ligand recoordination is rapid compared to ET in the pentacoordinated state [44]. Furthermore, water binding to the ferric (but not ferrous) pentacoordinate iron can attenuate reduction kinetics of the non *bis*–histidine state by increasing the nuclear reorganization energy associated with ET [45].

3.2 O_2 binding and PTM inhibition

S*ynechococcus* GlbN and GlbN-A, along with the closely related *Synechocystis* protein, undergo a large conformational change upon switching between *bis*–histidine and exogenous ligand-bound states [8, 46] (Figure S1A). In the cyanide-bound structure (Fe^{III}–CN^{-}), which serves as a model for the Fe^{II}–O_2 state, a distinct array of amino acids interacts with the distal ligand. The conserved Tyr22 OηH is the donor in an H-bond to the cyanide nitrogen; additionally, Gln43 and Gln47 NεH_2 groups are positioned to form a network of H-bonds with bound cyanide and Tyr22 Oη. These same interactions are thought to stabilize activated O_2 and inhibit dissociation or autooxidation [47, 48]. Dioxygen binding and activation to the ferric-superoxide species is shown in Equation 2.

$$\text{His70} - \text{Fe}^{\text{II}} + O_2 \leftrightarrows [\text{His70} - \text{Fe}^{\text{III}} - O_2^{-}] \quad (2)$$

Figure 1 illustrates O_2 binding by GlbN under oxic conditions where $[O_2] \gg [\text{GlbN}]$, as pertinent for optical absorbance spectrophotometry of air-equilibrated solutions. The

experiment makes use of Fd as an electron shuttle and an enzymatic reduction system to produce GlbN in the Fe^{II} state. Following mixing of the components, slow Fd-mediated reduction of GlbN is followed by rapid O_2 binding resulting in an apparent $Fe^{III} \rightarrow Fe^{II}–O_2$ transition (Figure 1A, dashed-line spectrum to solid-line spectrum). Useful absorption maxima are listed in Table 1.

In the absence of oxygen and at neutral pH, reduction of Fe^{III} GlbN to the Fe^{II} state is followed by PTM [14, 49]. The modification proceeds to completion within a few seconds. Under oxic conditions, however, the $Fe^{II}–O_2$ GlbN species (Figure 1B, solid-line spectrum) persists and shows no evidence of conversion to $Fe^{II}–O_2$ GlbN-A (Figure 1B, dash-dot spectrum) over 30 min. These observations are consistent with the inhibitory effect of O_2 toward the PTM and the detection of unmodified GlbN in synechococcal cells grown under oxic conditions.

3.3 NOD activity

Because the oxy form of GlbN and GlbN-A could be produced separately, we next compared their ability to catalyze the NO dioxygenation reaction, which is an accepted route for NO destruction by Hbs under oxic conditions [50]. Indeed, NO dioxygenase (NOD) activity in vivo has been proposed for TrHb1s from strains of *Mycobacterium* [51–53], the ciliate *Tetrahymena pyriformis* [48], microalgal raphidophytes (*Heterosigma akashiwo* and *Chattonella subsalsa*) [54], and the green alga *C. reinhardtii* [30]. The physiological evidence gathered so far does not rule out a similar role for GlbN and GlbN-A.

Beyond Equation 1a, the NOD reaction is a multi-step process [50] starting with O_2 binding (Equation 2) and proceeding with Equations 3a–b,

$$[\text{His70} – \text{Fe}^{\text{III}} – \text{O}_2^{-}] + \text{NO} \rightarrow [\text{His70} – \text{Fe}^{\text{III}} – \text{OONO}^{-}] \quad (3a)$$

$$[\text{His70} – \text{Fe}^{\text{III}} – \text{OONO}^{-}] \rightarrow \text{His70} – \text{Fe}^{\text{III}} + \text{NO}_3^{-} \quad (3b)$$

where process (3b) captures the steps of peroxynitrite isomerization [55]. To undergo NOD turnover, the resulting ferric protein must be re-reduced according to Equation 1b or 1c.

The reaction of GlbNs with NO under oxic conditions was examined with an optical assay developed in prior studies of *C. reinhardtii* THB1 [30]. Figure 2 presents the α–β region of the spectrum and intensity of the β band in representative experiments. Panel A illustrates the reaction with GlbN. The assay begins with *bis*–histidine Fe^{III} GlbN in the presence of the Fd/FNR reduction system but without NADPH (top dashed-line trace). Addition of NADPH results in the formation of $Fe^{II}–O_2$ GlbN (top solid trace). Monitoring the absorbance at 550 nm (Figure 2, inset) highlights the appearance of the characteristic β band of $Fe^{II}–O_2$ GlbN. Once the conversion to oxy GlbN is complete, the NO releasing agent MAHMA-NONOate is added (upper asterisk in inset). The spectral intensity associated with $Fe^{II}–O_2$ GlbN immediately begins to drop. Within 2 to 3 min, the entire sample is converted

to the Fe^{III} *bis*–histidine state (lower asterisk in inset). This ferric spectrum persists while the release of NO by MAHMA-NONOate and its consumption by regenerated Fe^{II}–O_2 GlbN continue. Upon depletion of NO, the protein returns to the Fe^{II}–O_2 GlbN state. These data are consistent with the O_2–binding observations presented above, with no build-up of *bis*–histidine Fe^{II} GlbN or production of GlbN-A.

Following each NO donor addition, the turnover period increased in duration, the extent of Fe^{II}–O_2 recovery was attenuated (decreasing solid traces), and the ferric state absorbance decreased over the whole spectrum (decreasing dashed-line traces), all indications of GlbN deactivation via heme bleaching. The $Fe^{III} \rightarrow Fe^{II}$–$O_2$ transition was also slower, an observation noted for all tested globins and attributed to NO poisoning of the Fd/FNR system. Addition of fresh Fd/FNR to the THB1 control sample (not shown) confirmed the interpretation. Panel B in Figure 2 presents the data for Fe^{II}–O_2 GlbN-A, which displays faster reduction and O_2 binding but undergoes more bleaching than GlbN on multiple NO additions. The deactivation observed for GlbNs is in contrast with the full recovery of THB1 [30] (Figure S2). Thus, GlbN and GlbN-A appear capable of NOD chemistry and may play such a role under oxic conditions, although heme damage suggests that they are not fit for multiple enzymatic turnovers, unlike THB1.

3.4 NO binding to Fe^{III} GlbN and GlbN-A

GlbN or GlbN-A may be able to manage endogenous NO concentration through O_2–independent mechanisms. In addition to sequestration, one possibility is reductive nitrosylation (or “autoreduction”) by which the ferric protein binds NO, forms the electrophilic Fe^{II}–NO^+ state, and eventually produces NO_2^- and ferrous protein under the action of OH^- or water [38, 56]. In the presence of excess NO, the ferrous protein is then converted to the Fe^{II}–NO state. Unlike horse skeletal myoglobin (Figure S3) and several other heme proteins [38, 56], treatment of ferric GlbN (or GlbN-A) with excess NO donor leads to stable $\{FeNO\}^6$ complexes (Figure 3), which were interrogated with NMR spectroscopy (Figures S4 and S5). Narrow ^1H chemical shift dispersion, sharp lines, and heme resonance assignments support that both Fe^{III}–NO complexes are diamagnetic ($S = 0$). Table 2 lists heme ^1H chemical shifts of Fe^{III}–NO GlbN and Fe^{III}–NO GlbN-A. Because both GlbN and GlbN-A were maintained in the ferric nitrosyl state for ~10 h, it seems unlikely that the NO elimination via the autoreduction process is relevant to their ability to protect *Synechococcus* from RNS/ROS.

3.5 Reduction of Fe^{III}–NO GlbN-A to Fe^{II}–NO GlbN-A

We next examined whether the Fe^{III}–NO GlbN-A complex could undergo forced reduction to the Fe^{II}–NO form. Fe^{III}–NO GlbN-A was prepared as above by treatment of the ferric protein with excess MAHMA-NONOate and monitored optically. Upon saturation with NO, the sample was reacted with excess DT, to make use of a relatively strong reducing agent [57]. Within the dead time of the experiment (~15 s), changes from the Fe^{III}–NO starting material (Figure 4A, dashed-line spectrum) were observed and suggested that reduction to a stable Fe^{II}–NO GlbN-A form (Figure 4A, solid-line spectrum) had occurred.

An analogous experiment was performed using an ^{15}N-labeled NMR sample of Fe^{III}–NO GlbN-A. Figure 4B shows the initial ^{1}H-^{15}N HSQC spectrum of Fe^{III}–NO GlbN-A (gray peaks). Although isoelectronic with Fe^{II}–CO GlbN-A, Fe^{III}–NO GlbN-A gave rise to a distinct ^{1}H-^{15}N correlation map, suggesting subtle structural differences between the two diamagnetic complexes. Reduction of Fe^{III}–NO GlbN-A with excess DT resulted in noticeable ^{1}H-^{15}N HSQC spectral changes (Figure 4B, black peaks). Despite the chemical shift perturbations, the NMR spectra are quite similar overall, and support that the ferric and ferrous nitrosyl forms share the same fold and mode of hexacoordination (His70–Fe–NO). However, in Fe^{II}–NO GlbN-A, the unpaired electron causes rapid paramagnetic relaxation for NH nuclei near the iron center and therefore broadens several signals beyond detection (e.g., the tentative His70 backbone amide in Fe^{III}–NO GlbN-A: ^{1}H = 5.55 ppm, ^{15}N = 106.3 ppm, is not observed in Fe^{II}–NO GlbN-A). These spectra, along with the lack of detectable heme signals in NOESY spectra, support that complete formation of paramagnetic (S = 1/2) Fe^{II}–NO GlbN-A had occurred.

3.6 The Fe^{II}–NO GlbN complex and NO reduction to HNO

The reduction behavior of ferric nitrosyl GlbN-A was used as a point of reference for GlbN experiments. As for GlbN-A, a Fe^{III}–NO GlbN sample was produced by treatment of the ferric protein with excess MAHMA-NONOate and monitored optically. Once saturation was achieved, excess DT was added to initiate reduction. Figure 5A shows representative results of the experiment. GlbN displayed distinct biphasic behavior compared to GlbN-A (Figure 4A). The first (rapid) phase was completed within ~3 min and was characterized by a marked decrease in Soret absorbance occurring concomitantly with a blue-shift (dash-dot spectrum); this initial rapid phase was followed by a slow ($t_{1/2}$ ~ 1 h) recovery phase (solid-line spectrum: 417 nm Soret, 559 nm merged α/β). The low Soret intensity and ~390 nm shoulder of the intermediate supported that formation of Fe^{II}–NO GlbN inhibited ferrous heme crosslinking and instead caused rapid heme dissociation. In agreement, similar biphasic spectral changes were detected upon DT reduction of Fe^{III}–NO H117A GlbN (a variant incapable of the His117–heme PTM).

NO can bind with pM affinity to ferrous heme [58] and is well known for its strong negative σ-*trans* effect [59]; the latter phenomenon can considerably weaken the coordination bond of the iron ligand on the other side of the heme plane. Indeed, the ~ 390 nm shoulder exhibited by the Fe^{II}–NO WT and H117A GlbNs intermediate is reminiscent of the blue-shifted Soret band (~ 398 nm) observed for the five-coordinate NO bound form(s) of the heme domain of soluble guanylate cyclase [60]. We examined the plausibility of weakened His70 coordination and lowered heme affinity by performing a heme transfer experiment. Fe^{III} GlbN was first incubated with an 8-fold molar excess of horse skeletal apomyoglobin; excess NONOate was then added as above (Figure 5A). The spectral changes that followed corresponded to formation of Fe^{III}–NO GlbN (Figure 5B, dashed-line trace). Upon completion, excess DT was added to initiate reduction. Following a 15-s dead time the distinctive optical signature of Fe^{II}–NO myoglobin was detected (Figure 5B, thin gray traces) in an indication of rapid heme acquisition. We therefore interpret the first phase observed upon DT reduction of Fe^{III}–NO GlbN (Figure 5A) as His70 deligation and heme dislodging.

To test the specific role of NO in promoting heme dissociation from ferrous GlbN, two additional heme transfer experiments were performed. In the first, ferric *bis*–histidine GlbN was reduced by DT in the presence of excess apomyoglobin. Under such conditions, we observed rapid formation of ferrous *bis*–histidine GlbN-A, and no detectable formation of deoxy Mb (Fe^{II} Mb) (Figure S6). Thus, uninhibited PTM clearly out-competes heme transfer near neutral pH. More importantly, when the ferrous carbonmonoxy state (Fe^{II}–CO GlbN) was generated in the presence of excess apomyoglobin (Figure S7), no heme transfer was detected over a period of 50 min. The CO result, in addition to the lack of detectable heme loss in Fe^{III}–NO GlbN, implicated specifically Fe^{II}–NO coordination as a causal factor for rapid heme dissociation in GlbN. In contrast to Fe^{II}–NO GlbN, the spectral features of the Fe^{II}–NO GlbN-A adduct are consistent with a stable six-coordinate His–Fe–NO complex, which indicates a proximal side of the heme cavity unable to accommodate a decoordinated His70, likely because of the crowding exerted by Met66, Leu73, and Val121.

^{1}H NMR was used to characterize the nature of the second phase and final product(s) in the reaction of Fe^{III}–NO GlbN with DT (Figure 5A, dash-dot to solid line transition). In this experiment, a concentrated Fe^{III}–NO GlbN solution (1.5 mM) was reduced with excess DT and allowed to incubate for ≥ 45 min prior to data acquisition. Unlike with GlbN-A, distinct diamagnetic forms were observed in the resulting mixture, and two ^{1}H signals (major and minor) reminiscent of nitrosyl hydride (HNO) within Fe^{II}–HNO myoglobin [61, 62] were detected at ~14.8 ppm (Figure 6A). Production of Fe^{II}–HNO from Fe^{III}–NO is summarized in the following reaction:

$$\text{His70} - \text{Fe}^{\text{III}} - \text{NO} + \text{H}^{+} + 2\text{e}^{-} \rightarrow \text{His70} - \text{Fe}^{\text{II}} - \text{HNO} \quad (4)$$

Under anoxic conditions, most Hbs can produce NO via nitrite reductase chemistry [21, 63–68]. This process is essentially the reverse of the autoreduction reaction described above and is initiated in the ferrous (deoxy) state. As an unambiguous test for DT-mediated HNO formation, we took advantage of the nitrite reductase activity of GlbN [21, 65] to produce nitric oxide in situ. Specifically, we incubated unlabeled Fe^{III} GlbN with ^{15}N-labeled nitrite ($^{15}NO_2^-$); excess DT was then added to initiate the reaction. Figure 6B shows the relevant region of the ^{1}H NMR spectrum following a ~ 2-h incubation. Compared with Figure 6A, the major (^{1}H = 14.82 ppm) and minor (^{1}H = 14.76 ppm) signals in Figure 6B are both split into doublets with $|^1J_{NH}|$ ~ 71 Hz; this result is consistent with formation of $H^{15}NO$. The magnitude of the $^1H^{15}NO$ $^1J_{NH}$–couplings were in good agreement with those determined previously for Fe^{II}–HNO Hb complexes ($|^1J_{NH}|$ = 66–72 Hz) [61, 69].

To explore the generality of the NO reduction chemistry, we tested whether H117A GlbN could also produce HNO. Figure 7A displays the ^{1}H NMR spectrum of H117A GlbN, treated with DT in the presence of $^{15}NO_2^-$ and allowed to recover for ~ 2 h. This variant is incapable of forming the heme PTM, and as observed for WT GlbN, a diamagnetic species with sharp lines was detected, which is inconsistent with Fe^{II}–NO H117A GlbN. Unlike the WT protein, however, a single ^{1}H doublet ($|^1J_{NH}|$ ~ 71 Hz), centered at ~ 14.9 ppm, was observed (Figure 7B). The doublet indicates that H117A GlbN is also able to produce $H^{15}NO$ from $^{15}NO_2^-$. The integrated intensity of the doublet relative to the resolved T80

amide suggested a ~ 36% Fe^{II}–HNO yield. ^{1}H-^{15}N HSQC 2-D spectra revealed the Fe^{II}–$H^{15}NO$ ^{15}N chemical shift to be ~536 ppm (Figure 7C) compared to ~580 ppm reported by others [69].

The minor peak (^{1}H = 14.76 ppm) detected in the WT spectra (Figure 6) likely corresponds to HNO trapped by Fe^{II} GlbN-A formed during the reduction procedure. In agreement with this interpretation, the minor peak was absent when using H117A GlbN (Figure 7). It is also worth reiterating that no HNO and only Fe^{II}–NO GlbN-A were detected when a pure WT GlbN-A sample was subjected to DT reduction in the presence of NO_2^- (and analogously, when Fe^{III}–NO GlbN-A was reduced with DT).

^{1}H-^{1}H NOESY and DQF-COSY spectra collected on Fe^{II}–HNO WT GlbN allowed for partial heme assignments and confirmed that both heme vinyl groups remained intact (Table 2). Therefore, upon NO or HNO binding, the spontaneous heme PTM was inhibited. Of note, an NOE between ^{1}HNO and the heme 8-methyl protons provides preliminary orientation information for the distal ligand and facilitates comparison with the detailed studies of HNO-myoglobin in which the HNO proton points toward the 1-methyl group [62].

The ability of GlbN to generate HNO was further examined by using a weaker reducing agent than DT. For this purpose, we turned to the NADPH-dependent diaphorase domain of *C. reinhardtii* NR, produced with only the FAD cofactor. This avoided the iron-sulfur cluster present in Fd, which could be affected by NO, and the heme present in the holodiaphorase, which could complicate interpretation. NADPH (~300 μM) present in solution was used to reduce the diaphorase flavin; it also allowed for the possibility of a hydride transfer mechanism to produce HNO (Fe^{III}–NO + $H^- \rightarrow$ Fe^{II}–HNO) [70].

Optical absorbance spectra monitoring the reactions of Fe^{III}–NO GlbN and Fe^{III}–NO GlbN-A with the heme-free diaphorase are shown in Figure 8. Reduction of Fe^{III}–NO GlbN-A resulted in relatively slow ($t_{1/2}$ ~ 5 min) formation of Fe^{II}–NO GlbN-A; upon addition of DT, only minimal changes were detected (Figure 8A). Addition of the diaphorase domain to Fe^{III}–NO GlbN caused a slow ($t_{1/2}$ ~ 10 min) conversion to a species attributable to Fe^{II}–NO GlbN (with heme only weakly associated). The spectral changes (decrease in Soret intensity, ~ 390 nm shoulder) were similar to those observed in the first phase following DT treatment (Figure 5A, dashed line to dash-dot line transition). The Fe^{II}–NO GlbN form could then be converted to Fe^{II}–HNO GlbN by addition of DT (Figure 8B). Thus, under the tested conditions, it appears that the diaphorase domain is not capable of providing the driving force necessary for Fe^{II}–HNO GlbN formation. The Fe^{II}–HNO state was also not detected when using the NADPH/diaphorase system to reduce H117A GlbN in the presence of nitrite (data not shown). These results support that NADPH was unable to reduce Fe^{III}–NO GlbN to the Fe^{II}–HNO form via direct hydride transfer.

Interestingly, subsequent optical absorbance experiments supported that the ability for GlbN but not GlbN-A to produce HNO is common to the *Synechocystis* GlbN/GlbN-A pair (Figure S8 and S9). In an experiment where Fe^{III} *Synechocystis* GlbN, excess nitrite, and excess DT were reacted, ^{1}H NMR spectra were used to positively identify the HNO proton (^{1}H = 14.80 ppm, data not shown). However, the yield of Fe^{II}–HNO in *Synechocystis* GlbN

(< 5 %) was considerably lower than that of the *Synechococcus* proteins (20–35 %). No such HNO signal was observed in the analogous experiment using *Synechocystis* GlbN-A.

4. Discussion

4.1 NOD activity of GlbN and GlbN-A

The current study supports that both oxy GlbN and oxy GlbN-A are capable of NOD activity. This in itself is not surprising as an increasing number of studies have implicated hemoglobins as a potential detoxifier of biologically produced NO [30, 50, 71]. Hargrove and coworkers have emphasized that single domain Hbs have dioxygenase activity in vitro, but are often limited by the reduction step in vivo [72]. As pointed out previously, the synechococcal cells contain an ample pool of reduced Fd [16], which as shown in our NOD assay can reliably reduce the heme. This would both eliminate the need for a dedicated reductase and link the activity of GlbN to a probable source of NO, the Fd-dependent nitrate reductase (NarB). In addition, the *bis*–histidine hexacoordination mode observed in GlbN and GlbN-A facilitates ET [49, 73, 74], which is a necessary step for NOD turnover (Equation 1c).

Upon multiple NO exposures, however, GlbN and GlbN-A undergo significant levels of heme damage. The bleaching effect may be due to release of peroxynitrite or nitrogen dioxide radical during the isomerization step [55]. Unlike the proposed role for the heme covalent modifications in mammalian heme peroxidases [75], the histidine–heme crosslink of GlbN does not appear to prevent this inactivation during catalytic activity. As the holoprotein is not resistant to the chemistry it catalyzes, it is unclear whether NOD is the main function of GlbN under oxic conditions. Perhaps the full complement of protective enzymes, including peroxiredoxins, acts to reduce the loss of activity. It is also possible that NOD-mediated damage of GlbN and GlbN-A serves as a signal for RNS/ROS stress in synechococcal cells, for example through tyrosine nitration [76, 77].

4.2 NO binding, heme dissociation, and a stabilization role for the PTM

Figure 3 shows that at high concentration, NO can displace an axial histidine of ferric *bis*–histidine GlbN and GlbN-A to form a His–Fe^{III}–NO complex. NMR data support that the proximal histidine remains coordinated while NO binds to the distal site and displaces His46, as CN^- does in the ferric state [8]. Unlike many heme proteins [38, 56, 72], Fe^{III}–NO GlbN and Fe^{III}–NO GlbN-A show negligible autoreduction to their Fe^{II}–NO forms over a timescale of several hours. We took advantage of this relative stability to initiate a preliminary NMR analysis of the diamagnetic Fe^{III}–NO complexes. We were able to assign heme ^1H resonances (Figure S4 and S5, Table 2) and acquire high-quality ^1H-^{15}N HSQC spectra (Figure 4B). Fe^{III}–NO GlbNs are therefore promising candidates for future NMR or resonance Raman studies that, for example, interrogate the interactions of bound NO with distal residues involved in the hydrogen bond network present in various TrHb1 complexes [8].

Although both GlbN and GlbN-A show a similar propensity for binding NO in the ferric state, the two proteins show marked differences with respect to their ability to form stable

{FeNO}^{7} complexes. Fe^{II} GlbN-A binds NO like many heme proteins [58, 78, 79]. In contrast, if Fe^{II} GlbN combines with NO prior to spontaneous histidine–heme crosslinking, the PTM is inhibited and the Fe^{II}–NO heme group dissociates with an estimated $k \geq 0.1\ s^{-1}$ (pH 7.1). Partial heme release is demonstrated by the heme-scavenging experiment (Figure 5B) and consistent with the absorbance spectrum of the ferrous nitrosyl GlbN complex formed by reaction with a relatively weak reductant (Figure 8B). This behavior is rationalized with a weakening of the proximal histidine Nε2–Fe coordination bond by the *trans* bonded NO and the formation of a five-coordinate/six-coordinate mixture. Regardless of the specific determinants, NO-mediated heme loss could potentially interfere with any enzymatic cycle involving ferrous iron, including NOD activity. Thus, we propose that the histidine–heme PTM in GlbNs is critical for stable Fe^{II}–NO binding.

4.3 NO reduction to HNO

Pentacoordinate ferrous hemoglobins are capable of binding HNO to form Fe^{II}–HNO adducts [61, 62, 69, 70, 80]. In a detailed NMR study of Fe^{II}–HNO myoglobin, Sulc and coworkers utilized NOE analysis and porphyrin ring current shifts, along with comparison to the Fe^{II}–CO form, to propose that an H-bond between the distal histidine (His64) Nε2–H and the HNO oxygen helps to stabilize the adduct [62]. Here, we have presented evidence that the *bis*–histidine GlbNs from *Synechococcus* and *Synechocystis* are also capable of trapping HNO (Figures 6, 7, and S9). Apparently, HNO can out-compete the endogenous distal ligand, His46, to bind the ferrous iron. Unlike Fe^{II}–HNO myoglobin produced under optimized conditions [61, 62], Fe^{II}–HNO GlbNs were marginally stable and allowed for only a preliminary NMR analysis. The maximal Fe^{II}–HNO GlbN yield, attained using the H117A variant, was ~36 %, at the low end of the pentacoordinate globin range (30–100 %, depending on the method used to form the HNO adduct and the specific protein [61, 69]). It is worth noting that HNO exchange between ferrous GlbN and ferrous GlbN-A is likely to occur, as evidenced by the formation of Fe^{II}–HNO GlbN-A, which is only detected in the presence of GlbN and not when starting with pure GlbN-A (Figure 6). Competition with the distal histidine for the iron may shift coupled equilibria to favor HNO dissociation and subsequent N_2O formation. Additionally, reduction of HNO to hydroxylamine or ammonia [81] and HNO/NO^- reaction with NO [82] (and residual O_2) present in solution provide additional outlets that may limit the Fe^{II}–HNO GlbN yield and lifetime.

The {FeNO}^{8} GlbN complexes have HNO ^{1}H chemical shifts that cluster around ~14.8 ppm (Figures 6 and 7, Table 2), a value within the range of those observed previously in Hbs (^{1}H ~ 14.6–15.6 ppm) [61, 69] and upfield from that of $[Fe^{II}–(CN)_5HNO]^{3-}$ (~20 ppm [83]) because of the porphyrin ring current. The ^{15}N chemical shift of HNO is upfield from reported values (536 ppm in GlbN, compared to ~580 ppm [69]), likely affected by differences in Fe^{II}–HNO bonding geometry. The ^{1}H-^{15}N J coupling ($|^1J_{NH}|$ ~ 71 Hz) observed for $^1H^{15}NO$ bound to ferrous GlbNs indicates that protonation occurs at the nitrogen and is in agreement with the splittings determined previously in Hbs ($|^1J_{NH}|$ ~ 66–72 Hz) and $[Fe^{II}–(CN)_5HNO]^{3-}$ ($|^1J_{NH}|$ ~ 71 Hz) [61, 69, 83, 84]. In the model complex (octaethylporphyrinato)5-Me-imidazole–Fe^{II}–HNO (or (OEP)Fe(HNO)(5-MeIm)), the proton chemical shift and ^{1}H-^{15}N splitting are slightly different: ^{1}H = 13.99 ppm and $|^1J_{NH}|$ = 77 Hz, which may be due to a solvent effect ($CDCl_3$ versus H_2O) and sample temperature

(253 K versus 298 K) [85]. Hydrogen bond interactions along with the heme Fe–N–H bond angle are also expected to influence HNO NMR parameters.

The ionization of free HNO in water occurs with a pK_a ~11.5 and involves a change in spin state (singlet HNO Δ H^+ + triplet NO^-) [82, 86]. By analogy with other metal-ligand complexes, it is expected that the pK_a value decreases when HNO is bound to iron. As a complicating factor, it is possible that NO^- bound to Fe^{II} GlbN adopts a singlet ground state [87] (singlet HNO Δ H^+ + singlet NO^-), which may increase its basicity above that of free HNO in water. We were able to detect the ^1H signal of HNO bound to WT Fe^{II} GlbN over a pH range of 7.0 to 9.2. However, the typical Fe^{II}–HNO yield was ~ 20% at neutral pH (Figure 6) and decreased to ~ 5% at pH 9.2 (data not shown). At basic pH, the decrease in HNO proton intensity could be due to deprotonation (partial formation of Fe^{II}–NO^-), enhanced base-catalyzed hydrogen exchange dynamics [84], or decreased formation/trapping efficiency (or any combination of factors). Still, the data provide a tentative apparent $pK_a \geq 8.5$ for HNO when bound to Fe^{II} GlbNs. This lower limit is below that of $[Fe^{II}–(CN)_5HNO]^{3-}$, which yielded a $pK_a \geq 11$ [84] as determined by the absence of pH-dependent changes in the HNO ^{17}O signal intensity and chemical shift.

The mechanism of NO reduction to HNO is of particular interest. Whereas DT was capable of reducing Fe^{III}–NO GlbN (or Fe^{III} GlbN + NO_2^-) to the Fe^{II}–HNO form, NADPH and the flavin bound diaphorase domain of NR produced only Fe^{II}–NO GlbN. Since the SO_2^- radical derived from DT homolysis is a one electron donor, the GlbN results suggest a sequential mechanism for HNO formation (Fe^{III}–NO + e^- → Fe^{II}–NO + e^- + H^+ → Fe^{II}–HNO, Figure S10), in which the second ET step is coupled to protonation. Reduction of a $\{FeNO\}^7$ complex to the $\{FeNO\}^8$ state by DT has precedents. For example, $[Fe^{II}–(CN)_5HNO]^{3-}$ can be produced from nitroprusside ion by sequential DT reduction at pH 10 [83]. Additionally, Poole and coworkers have demonstrated that the *E. coli* flavohemoglobin Hmp is capable of consuming NO (and producing N_2O) under anoxic conditions [88]. Because excess reductant was not required for the reaction, they postulated that NO reduction and NO^-/HNO release occurred spontaneously (Fe^{II}–NO → Fe^{III} + NO^-) [88].

Our results support that the mechanism of nitric oxide reduction in GlbNs is distinct from that of the dedicated enzyme, cytochrome P450nor. In P450nor, NADH (or borohydride) reduces the Fe^{III}–NO complex to “intermediate I” (Soret ~ 444 nm), presumably generating a transient Fe^{II}–HNO species which then undergoes protonation at the HNO oxygen [89–92]. In the presence of excess NO, intermediate I (proposed to be Fe^{IV}–HNOH) then reacts rapidly to produce N_2O and H_2O [89]. Notably, DT treatment of Fe^{III}–NO P450nor results only in formation of the Fe^{II}–NO state [89]. Similarly, the model HNO–heme (OEP)Fe(HNO)(5-MeIm) was produced by borohydride treatment of the $\{FeNO\}^6$ complex (Fe^{II}–NO^+ + H^- → Fe^{II}–HNO) [85]. Borohydride was also shown to be capable of reducing nitroprusside ion to $[Fe^{II}–(CN)_5HNO]^{3-}$ [70]. Indeed, the robustness of hydride transfer as a path to HNO production was demonstrated by Kumar and coworkers [70]: using the HNO scavengers Ni^{II} tetracyanate and Fe^{II} *N*–methyl-D-glucaminedithiocarbamate, they provided evidence that borohydride, but not DT, can reduce free nitrite to HNO (HONO + H^- → HNO + OH^-). The direct one-electron reduction of NO to triplet NO^- is highly unfavorable (estimated E°’ ~ −0.8 V vs. NHE [82, 86] at 1 M NO in aqueous solution) even when

considering the use of DT as a powerful reducing agent [57]. However, at neutral pH, protonation of triplet NO^- to singlet HNO is thermodynamically favored. Bartberger and coworkers demonstrated a pH-dependence to NO reduction in solution and estimated that proton-coupled reduction of NO to HNO at pH 7.2 would increase the E°' to about −0.5 V vs. NHE [86]. Farmer and coworkers have shown the electrochemical reduction of Fe^{II}–NO myoglobin occurs at −0.63 V vs. NHE at pH 10 [93]. Near neutral pH and at a concentration of ~1 mM, the effective reduction potential for DT is ~ −0.48 V [57], which is apparently sufficient for reduction of Fe^{II}–NO GlbN to the Fe^{II}–HNO state.

The reason that GlbN but not GlbN-A can generate HNO is not obvious, as the two proteins have comparable Fe^{III}/Fe^{II} reduction potentials in their *bis*–histidine forms [49], a similarity that may be expected to extend to the Fe^{II}–NO^+/Fe^{II}–NO and Fe^{II}–NO/Fe^{II}–NO^- couples. Nevertheless, the differential reactivity points toward a role for GlbN in HNO production, as opposed to, for example, DT reduction of free NO followed by trapping of HNO to the iron center (the latter would be expected to occur indiscriminately in the presence of GlbN and GlbN-A). We speculate that in the low affinity Fe^{II}–NO state of GlbN, His70 decoordination may alter the electrostatic environment of the iron and facilitate NO reduction to HNO (Figure S10). Additionally, differences in hydrogen bonding could alter the propensity for NO reduction. For example, H-bonding to the proximal nitrogen of Fe^{II}–NO has been proposed to bias the electron density of the $\{FeNO\}^7$ adduct in such a way as to promote HNO formation [94]. The intermediate Fe^{II}–NO GlbN complex is of interest for its ability to activate NO for reduction and is accessible for future mechanistic studies using a gentle reductant such as the flavin-containing diaphorase NR domain (Figure 8B).

Interest in HNO arises from its potential biomedical uses [95] and, relevant to cyanobacteria, as a source of N_2O [82]. The slow kinetics of Fe^{II}–HNO GlbN formation (Figure 5A) suggest that this chemistry is not important in vivo. Furthermore, the low reduction potential required to produce Fe^{II}–HNO GlbN from Fe^{II}–NO (E°' ~ −0.48 V) may be beyond what is accessible physiologically [96]. As mentioned above, bona fide mono-heme NO reductases such as cytochrome P450nor bypass the thermodynamic "dead-end" $\{FeNO\}^7$ state by using a distinct hydride transfer mechanism [89]. Although we did not observe such a reaction in vitro, we cannot rule out that *Synechococcus* contains a reductase capable of bypassing $\{FeNO\}^7$ GlbN in an analogous manner. Future work will examine the plausibility and potential consequences of GlbN-mediated endogenous HNO production in cyanobacteria.

5. Conclusions

Our exploration of the chemistry of GlbN and GlbN-A has revealed interesting features related to the management of ROS/RNS. Unlike the ferrous deoxy state, in which the spontaneous PTM occurs readily to produce GlbN-A, under excess O_2 conditions, ferrous GlbN rapidly forms an oxy complex and tends to maintain its *b* heme in the unmodified state. These in vitro results help to explain why GlbN is primarily obtained from *Synechococcus* cells grown under oxic conditions whereas GlbN-A is recovered from cells grown microoxically. GlbN and GlbN-A both perform the NO dioxygenase reaction; however, heme bleaching during multiple turnovers casts some doubt on this activity being the only one of functional relevance. If NO is able to outcompete O_2 in binding to ferrous

GlbN, the Fe^{II}–NO heme is rapidly dislodged from its cavity and HNO can be formed if a suitable reductant (e.g., DT) is available. Notably, we propose that the mechanism of HNO formation occurs through sequential ET events. NO-mediated heme dissociation and HNO production were also observed for *Synechocystis* GlbN. In contrast to GlbN, GlbN-A does not convert NO to HNO under similar conditions. In addition, the His117–heme covalent linkage in GlbN-A prevents Fe^{II}–NO heme loss and may be biologically important to prevent destructive reactions in the cytosol catalyzed by free heme. Whether the differential reactivity between GlbN and GlbN-A toward NO extends to other cyanobacterial GlbNs cannot be predicted at this time, although it is interesting that many such proteins contain a histidine at the analogous position of His117 and therefore may undergo the PTM. The heme-protein crosslink affords the ability to discriminate chemistries (HNO formation, heme loss) on the basis of the availability of a set of inhibitory heme ligands (NO, O_2, CO). Thus, GlbN illustrates a versatile system for the management of NO and other RNS and is a convenient model protein for the study of HNO chemistry.

Supplementary Material

Refer to Web version on PubMed Central for supplementary material.

Acknowledgement

This work was supported by the National Science Foundation Grant MCB-1330488. The authors thank Dr. John Toscano for helpful discussions regarding the chemistry of HNO. Lukas Gilevicius is acknowledged for his contributions in developing the NOD assay and Dr. Ananya Majumdar for NMR assistance. All authors declare no competing financial interest.

Abbreviations:

1-D	one-dimensional
2-D	two-dimensional
DH	dehydrogenase
DPTA	dipropylenetriamine
DQF-COSY	double-quantum filtered correlation spectroscopy
DT	dithionite
ET	electron transfer
FAD	flavin adenine dinucleotide
Fd	ferredoxin
FNR	ferredoxin-$NADP^+$ reductase
GlbN	*Synechococcus* sp. PCC 7002 or *Synechocystis* sp. PCC 6803 hemoglobin
GlbN-A	GlbN with His117–heme covalent attachment

GODCAT	glucose oxidase/D-glucose/catalase
Hb	hemoglobin
HNO	nitrosyl hydride
HSQC	heteronuclear single quantum coherence
MAHMA	methylamine hexamethylene methylamine
Mb	myoglobin
NOD	nitric oxide dioxygenase
NOE	nuclear Overhauser effect
NOESY	nuclear Overhauser effect spectroscopy
NR	nitrate reductase
(OEP)Fe(HNO)(5-MeIm)	(octaethylporphyrinato)5-Me-imidazole–Fe^{II}–HNO
PTM	posttranslational modification
RNS	reactive nitrogen species
ROS	reactive oxygen species
THB1	*Chlamydomonas reinhardtii* truncated hemoglobin 1
TOCSY	totally correlated spectroscopy
TrHb1	group 1 truncated hemoglobin
WT	wild-type

References

[1]. Prescott C, Bottle SE. Biological relevance of free radicals and nitroxides. Cell Biochem. Biophys 75 (2017) 227–240. [PubMed: 27709467]

[2]. Valko M, Leibfritz D, Moncol J, Cronin MTD, Mazur M, Telser J. Free radicals and antioxidants in normal physiological functions and human disease. Int. J. Biochem. Cell Biol 39 (2007) 44–84. [PubMed: 16978905]

[3]. Jeandroz S, Wipf D, Stuehr DJ, Lamattina L, Melkonian M, Tian ZJ, Zhu Y, Carpenter EJ, Wong GKS, Wendehenne D. Occurrence, structure, and evolution of nitric oxide synthase-like proteins in the plant kingdom. Sci. Signal 9 (2016) 9.

[4]. Torres MJ, Simon J, Rowley G, Bedmar EJ, Richardson DJ, Gates AJ, Delgado MJ. Nitrous oxide metabolism in nitrate-reducing bacteria: Physiology and regulatory mechanisms. in: Poole RK (Ed.), Advances in Bacterial Electron Transport Systems and Their Regulation, vol. 68, Advances in Microbial Physiology, Academic Press Ltd-Elsevier Science Ltd, London, 2016, pp. 353–432.

[5]. Poole RK. Nitric oxide and nitrosative stress tolerance in bacteria. Biochem. Soc. Trans 33 (2005) 176–180. [PubMed: 15667299]

[6]. Scott NL, Falzone CJ, Vuletich DA, Zhao J, Bryant DA, Lecomte JTJ. The hemoglobin of the cyanobacterium *Synechococcus* sp. PCC 7002: Evidence for hexacoordination and covalent adduct formation in the ferric recombinant protein. Biochemistry 41 (2002) 6902–6910. [PubMed: 12033922]

[7]. Pond MP, Majumdar A, Lecomte JTJ. Influence of heme post-translational modification and distal ligation on the backbone dynamics of a monomeric hemoglobin. Biochemistry 51 (2012) 5733–5747. [PubMed: 22775272]

[8]. Wenke BB, Lecomte JTJ, Heroux A, Schlessman JL. The 2/2 hemoglobin from the cyanobacterium *Synechococcus* sp. PCC 7002 with covalently attached heme: comparison of X-ray and NMR structures. Proteins 82 (2014) 528–534. [PubMed: 23999883]

[9]. Vu BC, Jones AD, Lecomte JTJ. Novel histidine-heme covalent linkage in a hemoglobin. J. Am. Chem. Soc 124 (2002) 8544–8545. [PubMed: 12121092]

[10]. Preimesberger MR, Wenke BB, Gilevicius L, Pond MP, Lecomte JTJ. Facile heme vinyl posttranslational modification in a hemoglobin. Biochemistry 52 (2013) 3478–3488. [PubMed: 23607716]

[11]. Rice SL, Preimesberger MR, Johnson EA, Lecomte JTJ. Introduction of a covalent histidine-heme linkage in a hemoglobin: A promising tool for heme protein engineering. J. Inorg. Biochem 141 (2014) 198–207. [PubMed: 25304367]

[12]. Vuletich DA, Falzone CJ, Lecomte JTJ. Structural and dynamic repercussions of heme binding and heme-protein cross-linking in *Synechococcus* sp. PCC 7002 hemoglobin. Biochemistry 45 (2006) 14075–14084. [PubMed: 17115702]

[13]. Nothnagel HJ, Love N, Lecomte JTJ. The role of the heme distal ligand in the post-translational modification of *Synechocystis* hemoglobin. J. Inorg. Biochem 103 (2009) 107–116. [PubMed: 18992944]

[14]. Nothnagel HJ, Preimesberger MR, Pond MP, Winer BY, Adney EM, Lecomte JTJ. Chemical reactivity of *Synechococcus* sp. PCC 7002 and *Synechocystis* sp. PCC 6803 hemoglobins: covalent heme attachment and bishistidine coordination. J. Biol. Inorg. Chem 16 (2011) 539–552. [PubMed: 21240532]

[15]. Das TK, Couture M, Ouellet Y, Guertin M, Rousseau DL. Simultaneous observation of the O–O and Fe–O_2 stretching modes in oxyhemoglobins. Proc. Natl. Acad. Sci. U. S. A 98 (2001) 479–484. [PubMed: 11209051]

[16]. Scott NL, Xu Y, Shen G, Vuletich DA, Falzone CJ, Li Z, Ludwig M, Pond MP, Preimesberger MR, Bryant DA, Lecomte JTJ. Functional and structural characterization of the 2/2 hemoglobin from *Synechococcus* sp. PCC 7002. Biochemistry 49 (2010) 7000–7011. [PubMed: 20669934]

[17]. Ludwig M, Bryant DA. Synechococcus sp. strain PCC 7002 transcriptome: Acclimation to temperature, salinity, oxidative stress, and mixotrophic growth conditions. Front. Microbiol 3 (2012) 354. [PubMed: 23087677]

[18]. Ludwig M, Chua TT, Chew CY, Bryant DA. Fur-type transcriptional repressors and metal homeostasis in the cyanobacterium Synechococcus sp. PCC 7002. Front. Microbiol 6 (2015) 1217. [PubMed: 26582412]

[19]. Sakamoto T, Inoue-Sakamoto K, Bryant DA. A novel nitrate/nitrite permease in the marine cyanobacterium *Synechococcus* sp. strain PCC 7002. J. Bacteriol 181 (1999) 7363–7372. [PubMed: 10572142]

[20]. Yamasaki H, Sakihama Y. Simultaneous production of nitric oxide and peroxynitrite by plant nitrate reductase: in vitro evidence for the NR-dependent formation of active nitrogen species. FEBS Lett 468 (2000) 89–92. [PubMed: 10683447]

[21]. Sturms R, DiSpirito AA, Hargrove MS. Plant and cyanobacterial hemoglobins reduce nitrite to nitric oxide under anoxic conditions. Biochemistry 50 (2011) 3873–3878. [PubMed: 21495624]

[22]. Radi R. Peroxynitrite, a stealthy biological oxidant. J. Biol. Chem 288 (2013) 26464–72642. [PubMed: 23861390]

[23]. Beckman JS, Koppenol WH. Nitric oxide, superoxide, and peroxynitrite: the good, the bad, and ugly. Am. J. Physiol 271 (1996) C1424–1437. [PubMed: 8944624]

[24]. Beckman JS, Beckman TW, Chen J, Marshall PA, Freeman BA. Apparent hydroxyl radical production by peroxynitrite: implications for endothelial injury from nitric oxide and superoxide. Proc. Natl. Acad. Sci. U. S. A 87 (1990) 1620–1624. [PubMed: 2154753]

[25]. Pryor WA, Squadrito GL. The chemistry of peroxynitrite: a product from the reaction of nitric oxide with superoxide. Am. J. Physiol 268 (1995) L699–722. [PubMed: 7762673]

[26]. Crack JC, Green J, Thomson AJ, Le Brun NE. Iron–sulfur clusters as biological sensors: The chemistry of reactions with molecular oxygen and nitric oxide. Acc. Chem. Res 47, American Chemical Society (2014) 3196–3205. [PubMed: 25262769]

[27]. Kharitonov VG, Sundquist AR, Sharma VS. Kinetics of nitrosation of thiols by nitric oxide in the presence of oxygen. J. Biol. Chem 270 (1995) 28158–28164. [PubMed: 7499306]

[28]. Zaffagnini M, De Mia M, Morisse S, Di Giacinto N, Marchand CH, Maes A, Lemaire SD, Trost P. Protein S-nitrosylation in photosynthetic organisms: A comprehensive overview with future perspectives. Biochim. Biophys. Acta 1864 (2016) 952–966. [PubMed: 26861774]

[29]. Scott NL, Lecomte JTJ. Cloning, expression, purification, and preliminary characterization of a putative hemoglobin from the cyanobacterium *Synechocystis* sp. PCC 6803. Protein Sci 9 (2000) 587–597. [PubMed: 10752621]

[30]. Johnson EA, Rice SL, Preimesberger MR, Nye DB, Gilevicius L, Wenke BB, Brown JM, Witman GB, Lecomte JTJ. Characterization of THB1, a *Chlamydomonas reinhardtii* truncated hemoglobin: linkage to nitrogen metabolism and identification of lysine as the distal heme ligand. Biochemistry 53 (2014) 4573–4589. [PubMed: 24964018]

[31]. Teale FWJ. Cleavage of heme-protein link by acid methylethylketone. Biochim. Biophys. Acta 35 (1959) 543. [PubMed: 13837237]

[32]. Fernandez E, Schnell R, Ranum LP, Hussey SC, Silflow CD, Lefebvre PA. Isolation and characterization of the nitrate reductase structural gene of *Chlamydomonas reinhardtii*. Proc. Natl. Acad. Sci. U. S. A 86 (1989) 6449–6453. [PubMed: 2475871]

[33]. Aliverti A, Curti B, Vanoni MA. Identifying and quantitating FAD and FMN in simple and in iron-sulfur-containing flavoproteins. Methods Mol. Biol 131 (1999) 9–23. [PubMed: 10494539]

[34]. Englander SW, Calhoun DB, Englander JJ. Biochemistry without oxygen. Anal. Biochem 161 (1987) 300–306. [PubMed: 3578795]

[35]. Hayashi A, Suzuki T, Shin M. An enzymic reduction system for metmyoglobin and methemoglobin, and its application to functional studies of oxygen carriers. Biochim. Biophys. Acta 310 (1973) 309–316. [PubMed: 4146292]

[36]. Keefer LK, Nims RW, Davies KM, Wink DA. “NONOates” (1-substituted diazen-1-ium-1,2-diolates) as nitric oxide donors: convenient nitric oxide dosage forms. Methods Enzymol 268 (1996) 281–293. [PubMed: 8782594]

[37]. Hrabie JA, Klose JR, Wink DA, Keefer LK. New nitric oxide-releasing zwitterions derived from polyamines. J. Org. Chem 58 (1993) 1472–1476.

[38]. Addison AW, Stephanos JJ. Nitrosyliron(III) hemoglobin: autoreduction and spectroscopy. Biochemistry 25 (1986) 4104–4113. [PubMed: 3741844]

[39]. Delaglio F, Grzesiek S, Vuister GW, Zhu G, Pfeifer J, Bax A. NMRPipe: a multidimensional spectral processing system based on UNIX pipes. J. Biomol. NMR 6 (1995) 277–293. [PubMed: 8520220]

[40]. Goddard TD, Kneller DG. SPARKY 3 University of California, San Francisco (2006).

[41]. Wishart DS, Bigam CG, Yao J, Abildgaard F, Dyson HJ, Oldfield E, Markley JL, Sykes BD. ^{1}H, ^{13}C and ^{15}N chemical shift referencing in biomolecular NMR. J. Biomol. NMR 6 (1995) 135–140. [PubMed: 8589602]

[42]. Enemark JH, Feltham RD. Principles of structure, bonding, and reactivity for metal nitrosyl complexes. Coord. Chem. Rev 13 (1974) 339–406.

[43]. Smagghe BJ, Sarath G, Ross E, Hilbert JL, Hargrove MS. Slow ligand binding kinetics dominate ferrous hexacoordinate hemoglobin reactivities and reveal differences between plants and other species. Biochemistry 45 (2006) 561–570. [PubMed: 16401085]

[44]. Preimesberger MR, Majumdar A, Lecomte JTJ. Dynamics of lysine as a heme axial ligand: NMR analysis of the *Chlamydomonas reinhardtii* hemoglobin THB1. Biochemistry 56 (2017) 551–569. [PubMed: 28032976]

[45]. Tsukahara K. Kinetics and mechanisms of reduction of metmyoglobins - Importance of the geometry change at the heme iron site upon reduction. J. Am. Chem. Soc 111 (1989) 2040–2044.

[46]. Trent JT, 3rd, Kundu S, Hoy JA, Hargrove MS. Crystallographic analysis of *Synechocystis* cyanoglobin reveals the structural changes accompanying ligand binding in a hexacoordinate hemoglobin. J. Mol. Biol 341 (2004) 1097–1108. [PubMed: 15289104]

[47]. Gardner AM, Martin LA, Gardner PR, Dou Y, Olson JS. Steady-state and transient kinetics of Escherichia coli nitric-oxide dioxygenase (flavohemoglobin). The B10 tyrosine hydroxyl is essential for dioxygen binding and catalysis. J. Biol. Chem 275 (2000) 12581–12589. [PubMed: 10777548]

[48]. Igarashi J, Kobayashi K, Matsuoka A. A hydrogen-bonding network formed by the B10-E7-E11 residues of a truncated hemoglobin from *Tetrahymena pyriformis* is critical for stability of bound oxygen and nitric oxide detoxification. J. Biol. Inorg. Chem 16 (2011) 599–609. [PubMed: 21298303]

[49]. Preimesberger MR, Pond MP, Majumdar A, Lecomte JTJ. Electron self-exchange and self-amplified posttranslational modification in the hemoglobins from *Synechocystis* sp. PCC 6803 and *Synechococcus* sp. PCC 7002. J. Biol. Inorg. Chem 17 (2012) 599–609. [PubMed: 22349976]

[50]. Gardner PR. Hemoglobin: A nitric-oxide dioxygenase. Scientifica 2012 (2012) 34.

[51]. Milani M, Pesce A, Ouellet H, Guertin M, Bolognesi M. Truncated hemoglobins and nitric oxide action. IUBMB Life 55 (2003) 623–627. [PubMed: 14711009]

[52]. Ascenzi P, Bolognesi M, Milani M, Guertin M, Visca P. Mycobacterial truncated hemoglobins: from genes to functions. Gene 398 (2007) 42–51. [PubMed: 17532149]

[53]. Pathania R, Navani NK, Gardner AM, Gardner PR, Dikshit KL. Nitric oxide scavenging and detoxification by the *Mycobacterium tuberculosis* haemoglobin, HbN in *Escherichia coli*. Mol. Microbiol 45 (2002) 1303–1314. [PubMed: 12207698]

[54]. Stewart JJ, Coyne KJ. Analysis of raphidophyte assimilatory nitrate reductase reveals unique domain architecture incorporating a 2/2 hemoglobin. Plant Mol. Biol 77 (2011) 565–575. [PubMed: 22038092]

[55]. Su J, Groves JT. Mechanisms of peroxynitrite interactions with heme proteins. Inorg. Chem 49 (2010) 6317–6329. [PubMed: 20666389]

[56]. Hoshino M, Maeda M, Konishi R, Seki H, Ford PC. Studies on the reaction mechanism for reductive nitrosylation of ferrihemoproteins in buffer solutions. J. Am. Chem. Soc 118 (1996) 5702–5707.

[57]. Mayhew SG. The redox potential of dithionite and SO_2^- from equilibrium reactions with flavodoxins, methyl viologen and hydrogen plus hydrogenase. Eur. J. Biochem 85 (1978) 535–547. [PubMed: 648533]

[58]. Tsai AL, Berka V, Martin E, Olson JS. A “sliding scale rule” for selectivity among NO, CO, and O2 by heme protein sensors. Biochemistry 51 (2012) 172–186. [PubMed: 22111978]

[59]. Traylor TG, Sharma VS. Why NO?, Biochemistry 31 (1992) 2847–2849. [PubMed: 1348002]

[60]. Stone JR, Marletta MA. Soluble guanylate cyclase from bovine lung: activation with nitric oxide and carbon monoxide and spectral characterization of the ferrous and ferric states. Biochemistry 33 (1994) 5636–5640. [PubMed: 7910035]

[61]. Lin R, Farmer PJ. The HNO adduct of myoglobin: synthesis and characterization. J. Am. Chem. Soc 122 (2000) 2393–2394.

[62]. Sulc F, Fleischer E, Farmer PJ, Ma D, La Mar GN. ^{1}H NMR structure of the heme pocket of HNO-myoglobin. J. Biol. Inorg. Chem 8 (2003) 348–352. [PubMed: 12589571]

[63]. Ascenzi P, Leboffe L, Pesce A, Ciaccio C, Sbardella D, Bolognesi M, Coletta M. Nitrite-reductase and peroxynitrite isomerization activities of Methanosarcina acetivorans protoglobin. PLoS One 9 (2014) e95391. [PubMed: 24827820]

[64]. Rassaf T, Flogel U, Drexhage C, Hendgen-Cotta U, Kelm M, Schrader J. Nitrite reductase function of deoxymyoglobin: oxygen sensor and regulator of cardiac energetics and function. Circ. Res 100 (2007) 1749–1754. [PubMed: 17495223]

[65]. Tiso M, Tejero J, Kenney C, Frizzell S, Gladwin MT. Nitrite reductase activity of nonsymbiotic hemoglobins from *Arabidopsis thaliana*. Biochemistry 51 (2012) 5285–5292. [PubMed: 22620259]

[66]. Tiso M, Tejero J, Basu S, Azarov I, Wang X, Simplaceanu V, Frizzell S, Jayaraman T, Geary L, Shapiro C, Ho C, Shiva S, Kim-Shapiro DB, Gladwin MT. Human neuroglobin functions as a redox-regulated nitrite reductase. J. Biol. Chem 286 (2011) 18277–18289. [PubMed: 21296891]

[67]. Gladwin MT, Kim-Shapiro DB. The functional nitrite reductase activity of the heme-globins. Blood 112 (2008) 2636–2647. [PubMed: 18596228]

[68]. Shiva S, Huang Z, Grubina R, Sun J, Ringwood LA, MacArthur PH, Xu X, Murphy E, Darley-Usmar VM, Gladwin MT. Deoxymyoglobin is a nitrite reductase that generates nitric oxide and regulates mitochondrial respiration. Circ. Res 100 (2007) 654–661. [PubMed: 17293481]

[69]. Kumar MR, Pervitsky D, Chen L, Poulos T, Kundu S, Hargrove MS, Rivera EJ, Diaz A, Colon JL, Farmer PJ. Nitrosyl hydride (HNO) as an O2 analogue: long-lived HNO adducts of ferrous globins. Biochemistry 48 (2009) 5018–5025. [PubMed: 19368336]

[70]. Kumar MR, Fukuto JM, Miranda KM, Farmer PJ. Reactions of HNO with heme proteins: New routes to HNO–heme complexes and insight into physiological effects. Inorg. Chem 49 (2010) 6283–6292. [PubMed: 20666387]

[71]. Ouellet H, Ouellet Y, Richard C, Labarre M, Wittenberg B, Wittenberg J, Guertin M. Truncated hemoglobin HbN protects *Mycobacterium bovis* from nitric oxide. Proc. Natl. Acad. Sci. U. S. A 99 (2002) 5902–5907. [PubMed: 11959913]

[72]. Smagghe BJ, Trent JT, 3rd, Hargrove MS. NO dioxygenase activity in hemoglobins is ubiquitous in vitro, but limited by reduction in vivo. PLoS ONE 3 (2008) e2039. [PubMed: 18446211]

[73]. Weiland TR, Kundu S, Trent JT, 3rd, Hoy JA, Hargrove MS. Bis-histidyl hexacoordination in hemoglobins facilitates heme reduction kinetics. J. Am. Chem. Soc 126 (2004) 11930–11935. [PubMed: 15382928]

[74]. Athwal NS, Alagurajan J, Sturms R, Fulton DB, Andreotti AH, Hargrove MS. Electron self-exchange in hemoglobins revealed by deutero-hemin substitution. J. Inorg. Biochem 150 (2015) 139–147. [PubMed: 26141377]

[75]. Huang L, Wojciechowski G, Ortiz de Montellano PR. Role of heme-protein covalent bonds in mammalian peroxidases. Protection of the heme by a single engineered heme-protein link in horseradish peroxidase. J. Biol. Chem 281 (2006) 18983–18988. [PubMed: 16651262]

[76]. Sawa T, Akaike T, Maeda H. Tyrosine nitration by peroxynitrite formed from nitric oxide and superoxide generated by xanthine oxidase. J. Biol. Chem 275 (2000) 32467–32474. [PubMed: 10906338]

[77]. Reiter CD, Teng RJ, Beckman JS. Superoxide reacts with nitric oxide to nitrate tyrosine at physiological pH via peroxynitrite. J. Biol. Chem 275 (2000) 32460–32466. [PubMed: 10906340]

[78]. Copeland DM, West AH, Richter-Addo GB. Crystal structures of ferrous horse heart myoglobin complexed with nitric oxide and nitrosoethane. Proteins 53 (2003) 182–192. [PubMed: 14517970]

[79]. Brucker EA, Olson JS, Ikeda-Saito M, Phillips GN, Jr. Nitric oxide myoglobin: crystal structure and analysis of ligand geometry. Proteins 30 (1998) 352–356. [PubMed: 9533619]

[80]. Sulc F, Immoos CE, Pervitsky D, Farmer PJ. Efficient trapping of HNO by deoxymyoglobin. J. Am. Chem. Soc 126 (2004) 1096–1101. [PubMed: 14746478]

[81]. Montenegro AC, Bari SE, Olabe JA. Reactivity of iron(II)-bound nitrosyl hydride (HNO, nitroxyl) in aqueous solution. J. Inorg. Biochem 118 (2013) 108–114. [PubMed: 23153690]

[82]. Shafirovich V, Lymar SV. Nitroxyl and its anion in aqueous solutions: spin states, protic equilibria, and reactivities toward oxygen and nitric oxide. Proc. Natl. Acad. Sci. U. S. A 99 (2002) 7340–7345. [PubMed: 12032284]

[83]. Montenegro AC, Amorebieta VT, Slep LD, Martin DF, Roncaroli F, Murgida DH, Bari SE, Olabe JA. Three redox states of nitrosyl: NO+, NO•, and NO-/HNO interconvert reversibly on the same pentacyanoferrate(II) platform. Angew. Chem. Int. Ed. Engl 48 (2009) 4213–4216. [PubMed: 19425036]

[84]. Gao Y, Toubaei A, Kong XQ, Wu G. Acidity and hydrogen exchange dynamics of iron(II)-bound nitroxyl in aqueous solution. Angew. Chem. Int. Ed. Engl 53 (2014) 11547–11551. [PubMed: 25205463]

[85]. Abucayon EG, Khade R.l.L., Powell DR, Zhang Y, Richter-Addo GB. Hydride attack on a coordinated ferric nitrosyl: Experimental and DFT evidence for the formation of a heme model–HNO derivative. J. Am. Chem. Soc 138 (2016) 104–107. [PubMed: 26678216]

[86]. Bartberger MD, Liu W, Ford E, Miranda KM, Switzer C, Fukuto JM, Farmer PJ, Wink DA, Houk KN. The reduction potential of nitric oxide (NO) and its importance to NO biochemistry. Proc. Natl. Acad. Sci. U. S. A 99 (2002) 10958–10963. [PubMed: 12177417]

[87]. Pellegrino J, Bari SE, Bikiel DE, Doctorovich FA. Successful stabilization of the elusive species $\{FeNO\}^8$ in a heme model. J. Am. Chem. Soc 132 (2010) 989–995. [PubMed: 20043668]

[88]. Kim SO, Orii Y, Lloyd D, Hughes MN, Poole RK. Anoxic function for the Escherichia coli flavohaemoglobin (Hmp): reversible binding of nitric oxide and reduction to nitrous oxide. FEBS Lett 445 (1999) 389–394. [PubMed: 10094495]

[89]. Shiro Y, Fujii M, Iizuka T, Adachi S, Tsukamoto K, Nakahara K, Shoun H. Spectroscopic and kinetic studies on reaction of cytochrome P450nor with nitric oxide. Implication for its nitric oxide reduction mechanism. J. Biol. Chem 270 (1995) 1617–1623. [PubMed: 7829493]

[90]. Daiber A, Nauser T, Takaya N, Kudo T, Weber P, Hultschig C, Shoun H, Ullrich V. Isotope effects and intermediates in the reduction of NO by $P450_{NOR}$. J. Inorg. Biochem 88 (2002) 343–352. [PubMed: 11897349]

[91]. Daiber A, Shoun H, Ullrich V. Nitric oxide reductase (P450nor) from Fusarium oxysporum. J. Inorg. Biochem 99 (2005) 185–193. [PubMed: 15598501]

[92]. Goodrich LE, Paulat F, Praneeth VK, Lehnert N. Electronic structure of heme-nitrosyls and its significance for nitric oxide reactivity, sensing, transport, and toxicity in biological systems. Inorg. Chem 49 (2010) 6293–6316. [PubMed: 20666388]

[93]. Bayachou M, Lin R, Cho W, Farmer PJ. Electrochemical reduction of NO by myoglobin in surfactant film: Characterization and reactivity of the nitroxyl (NO-) adduct. J. Am. Chem. Soc 120 (1998) 9888–9893.

[94]. Xu CL, Spiro TG. Ambidentate H-bonding by heme-bound NO: structural and spectral effects of -O versus -N H-bonding. J. Biol. Inorg. Chem 13 (2008) 613–621. [PubMed: 18274790]

[95]. Flores-Santana W, Salmon DJ, Donzelli S, Switzer CH, Basudhar D, Ridnour L, Cheng R, Glynn SA, Paolocci N, Fukuto JM, Miranda KM, Wink DA. The specificity of nitroxyl chemistry is unique among nitrogen oxides in biological systems. Antioxid. Redox Signal 14 (2011) 1659–1674. [PubMed: 21235346]

[96]. Bottin H, Lagoutte B. Ferrodoxin and flavodoxin from the cyanobacterium *Synechocystis* sp PCC 6803. Biochim. Biophys. Acta 1101 (1992) 48–56. [PubMed: 1633177]

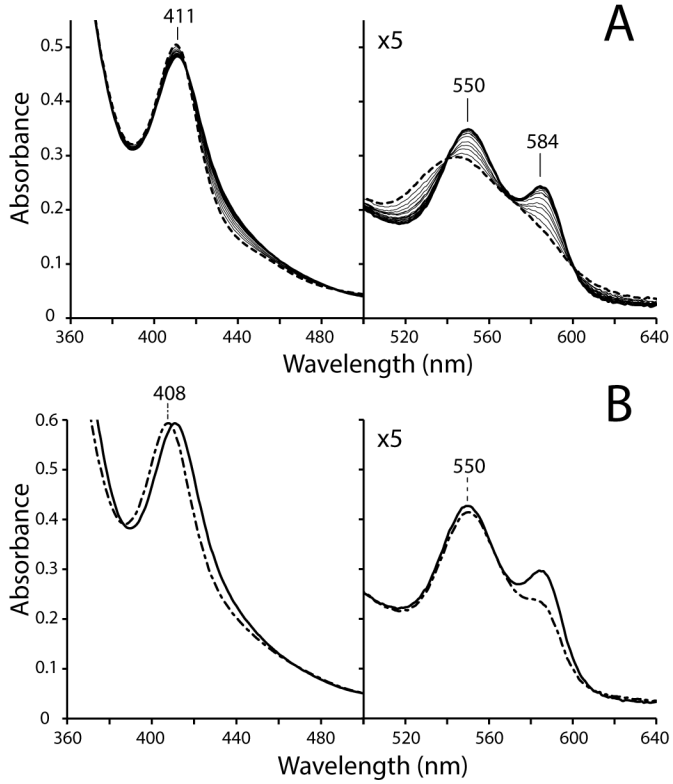

Fig. 1.

(A) Dioxygen binding monitored by optical absorbance spectrophotometry. A ~5.4 μM ferric GlbN sample at pH 7.1 (Fe^{III}, dashed trace) was incubated with a catalytic ferredoxin (Fd) reduction system. Gradual conversion of Fe^{III} GlbN to oxy GlbN (Fe^{II}–O_2) occurred in 10 min (solid traces). (B) Spectral overlay of Fe^{II}–O_2 GlbN (solid trace) and Fe^{II}–O_2 GlbN-A (dash-dot trace) prepared with the Fd reduction system.

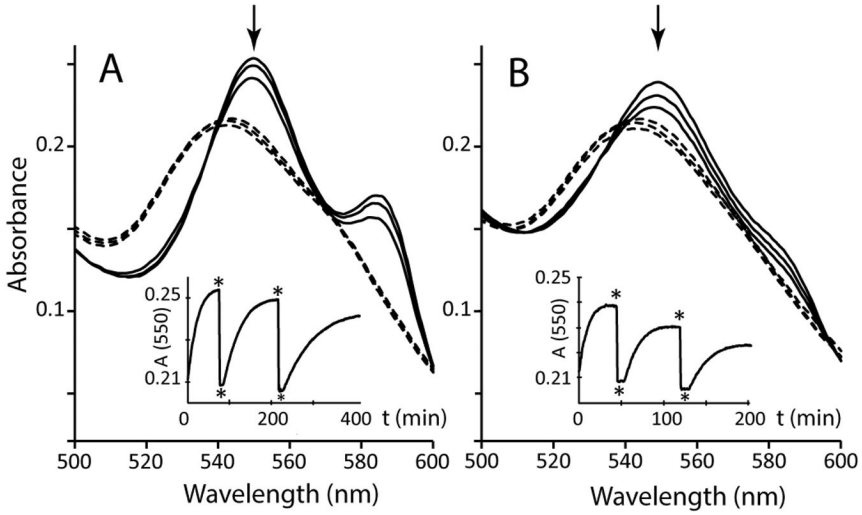

Fig. 2.

NOD assay performed with (A) ~20 μM GlbN or (B) ~20 μM GlbN-A (50 mM Tris, pH 7.2). The Fe^{III} *bis*–histidine proteins (most intense of the dashed-line spectra) were incubated with Fd and FNR; 300 μM NADPH was then added to initiate the reactions. (A) Following reduction and dioxygen binding, Fe^{II}–O_2 GlbN (most intense of the solid-line spectra) was treated with 15 μM of MAHMA-NONOate. Rapid oxidation to Fe^{III} *bis*–histidine GlbN followed (middle dashed-line spectrum) and this state persisted for ~6 min during turnover. Return to the Fe^{II}–O_2 state occurred after NO consumption (middle solid-line spectrum). A second NONOate addition yielded the lowest intensity Fe^{III} *bis*–histidine GlbN and Fe^{II}–O_2 GlbN spectra. The inset presents the response at 550 nm (arrow). Upper asterisks indicate NO donor addition and lower asterisks mark the turnover periods. (B) Data of the same acquired on GlbN-A. Note the different x-axis in the inset.

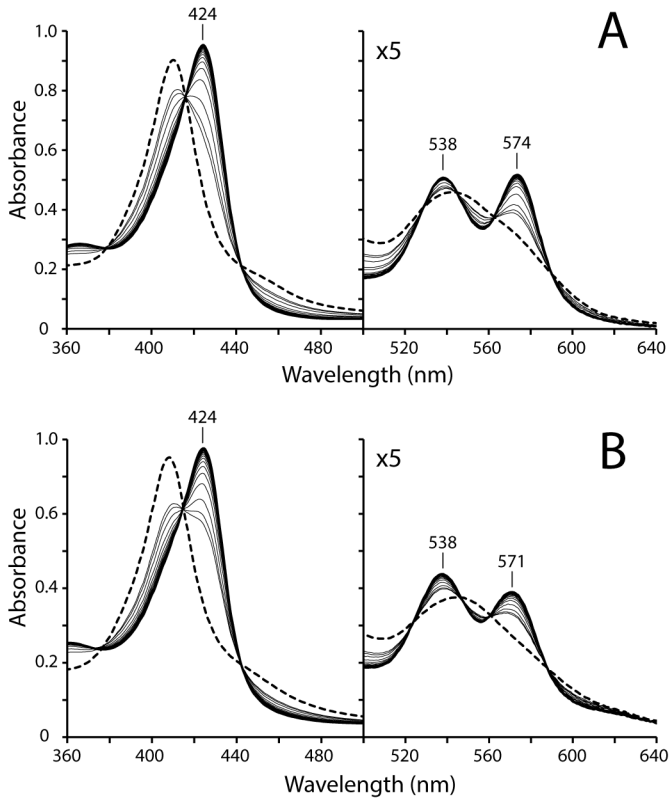

Fig. 3.

Formation of Fe^{III}–NO GlbN and GlbN-A. Approximately 1.3 mM MAHMA-NONOate was added to a sample of ~9 μM (A) Fe^{III} *bis*–histidine GlbN or (B) Fe^{III} *bis*–histidine GlbN-A (~100 mM phosphate, pH 7.1, dashed-line spectra). Conversion to the ferric NO adducts (solid-line spectra, acquired ~15 min after NONOate addition) was monitored over time (thin solid-line spectra).

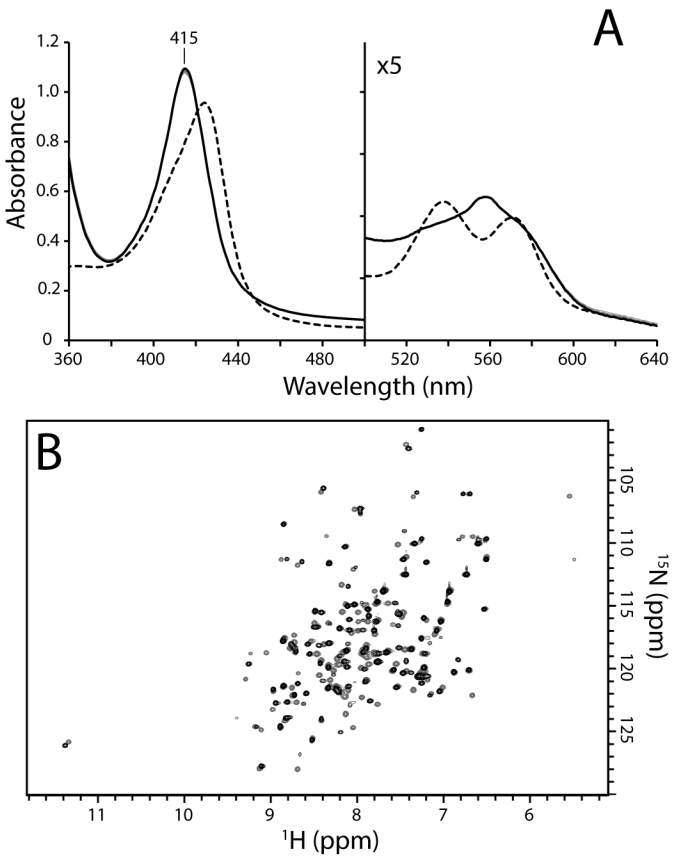

Fig. 4.

Reduction of Fe^{III}–NO GlbN-A using DT. (A) Dashed-line spectrum: Fe^{III}–NO GlbN-A obtained by treatment of Fe^{III} *bis*–histidine GlbN-A (~9 μM, GODCAT, 100 mM phosphate, pH 7.1) with 0.8 mM MAHMA-NONOate. Solid-line spectrum: Fe^{II}–NO GlbN-A, 10 min after addition of 2 mM DT; the band at ~558 nm is due to the presence of a small fraction of Fe^{II} *bis*–histidine GlbN-A. Thin gray traces: spectra acquired between the 15 s dead time and 10 min (every 30 s) showing that formation of Fe^{II}–NO GlbN-A occurred almost entirely during the dead time. (B) Overlay of ^{1}H-^{15}N HSQC spectra acquired on Fe^{III}–NO GlbN-A (gray or red) and Fe^{II}–NO GlbN-A (black). Fe^{III}–NO GlbN-A (~850 μM GlbN, 250 mM phosphate, pH 7.2, 10% D_2O) was prepared by addition of ~5 mM DPTA-NONOate to the Fe^{III} *bis*–histidine protein in the presence of GODCAT. The spectrum of Fe^{III}–NO GlbN-A was acquired ~5 h following NONOate addition. Fe^{II}–NO GlbN-A was prepared from the Fe^{III}–NO GlbN-A sample by addition of 8 mM DT under an argon atmosphere.

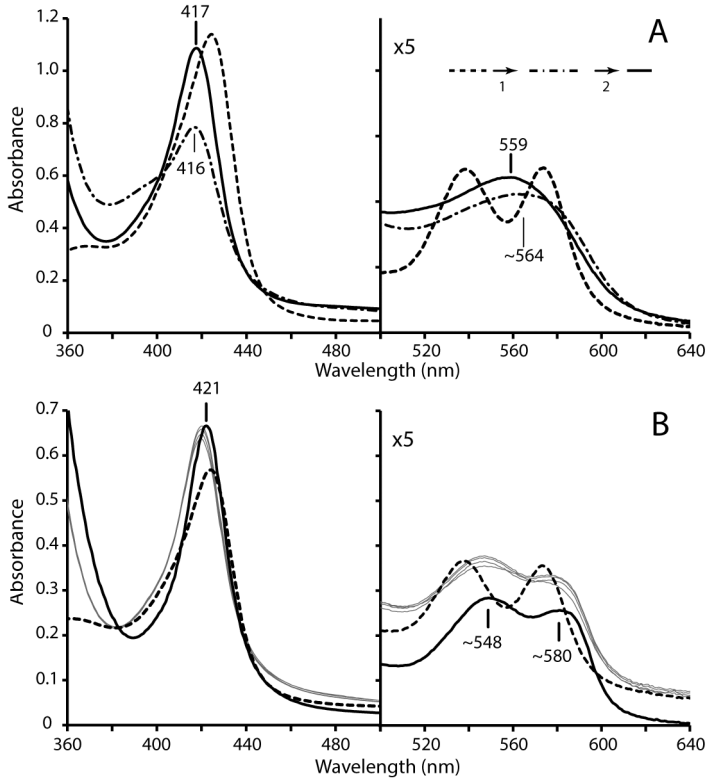

Fig. 5.

Reduction of Fe^{III}–NO GlbN (~10 μM, GODCAT, 100 mM phosphate, pH 7.1) using DT. (A) Dashed-line spectrum: Fe^{III}–NO GlbN obtained by treatment of Fe^{III} *bis*–histidine with 0.8 mM MAHMA-NONOate. Dash-dot spectrum: the mixture obtained ~3 min after DT addition. Solid-line spectrum: the mixture obtained ~200 min after DT reduction. (B) DT reduction of Fe^{III}–NO GlbN (~5 μM, GODCAT, 100 mM phosphate, pH 7.1) in the presence of ~40 μM apomyoglobin. Dashed-line spectrum: Fe^{III}–NO GlbN obtained by treatment of Fe^{III} *bis*–histidine with 1.6 mM MAHMA-NONOate in the presence of apomyoglobin. The increased baseline absorbance is indicative of Rayleigh scattering. Thin gray spectra: species obtained immediately after DT addition. The intensity increases slightly over a few min. Solid-line spectrum: Fe^{II}–NO myoglobin prepared by DT reduction of ferric myoglobin in the presence of nitrite.

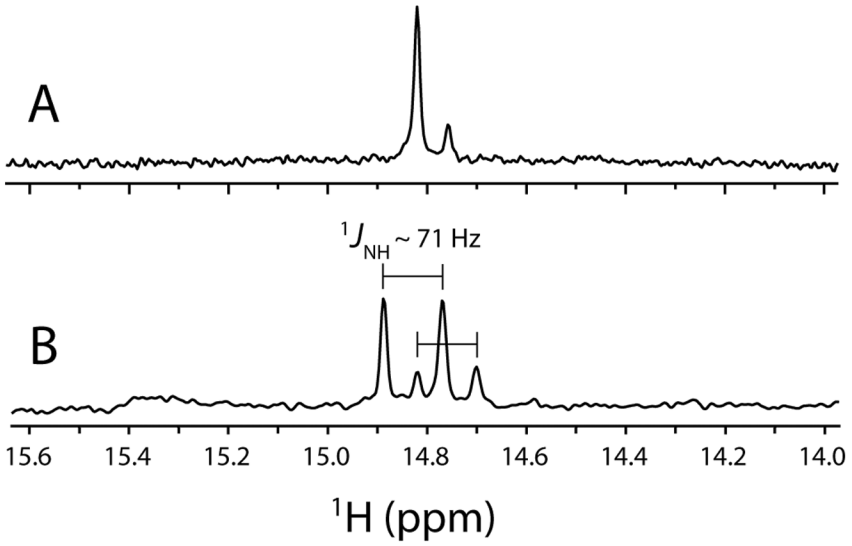

Fig. 6.

Downfield region of ^{1}H NMR spectra of Fe^{II}–HNO WT GlbN. (A) A 1.5 mM Fe^{III} *bis*–histidine WT ^{15}N GlbN sample (200 mM phosphate, pH 7.1, 10% D_2O, 298 K, GODCAT) was treated with 7.5 mM MAHMA-NONOate. The resulting mixture of Fe^{III} *bis*–histidine and Fe^{III}–NO GlbN was then treated with 7.5 mM DT. After ~ 50 min incubation, two Fe^{II}–HNO signals are detected (with major:minor intensity ratio ~ 4:1). The total HNO yield was estimated by peak integration to be ~ 23 %. (B) A 400 μM Fe^{III} *bis*–histidine WT GlbN sample (70 mM phosphate, pH 8.5 (pre DT), 10% D_2O, 298 K, GODCAT) incubated with 5 mM ^{15}N-nitrite was treated with 5 mM DT. After a ~ 2 h incubation, two $H^{15}NO$ doublets, each split by $^1J_{NH}$ = 71 Hz, were observed and correspond to Fe^{II}–$H^{15}NO$ GlbN (major signals) and Fe^{II}–$H^{15}NO$ GlbN-A (minor signals). The total $H^{15}NO$ yield was estimated by peak integration to be ~ 21 %.

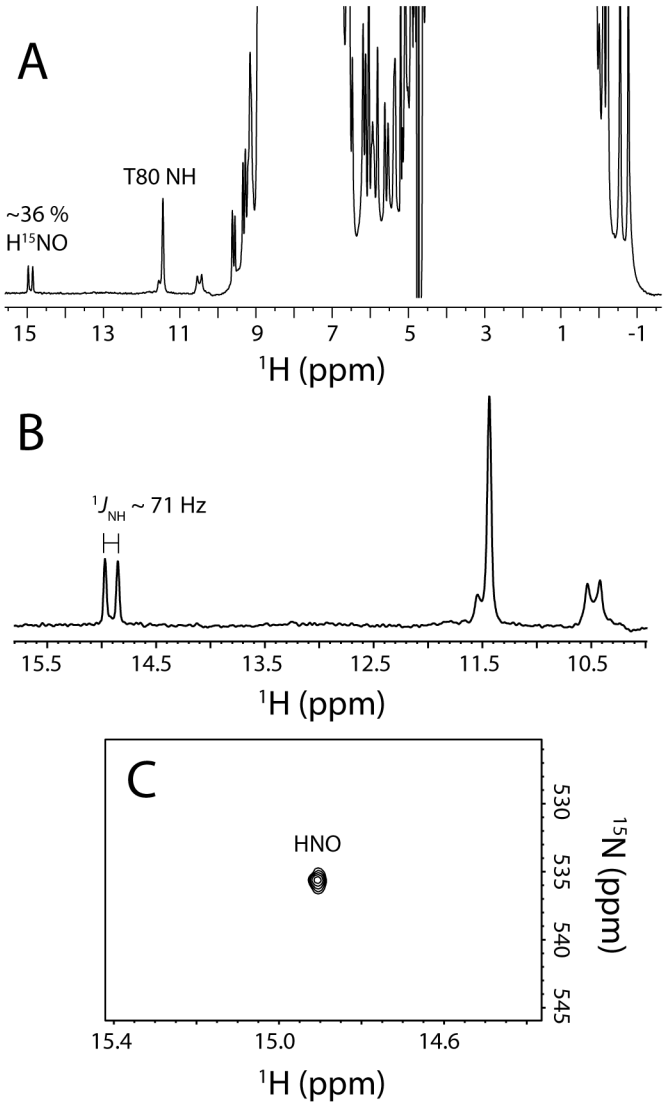

Fig. 7.

^{1}H and ^{15}N NMR evidence for Fe^{II}–HNO formation in H117A GlbN. (A) The ^{1}H NMR spectrum of an ~850 μM ^{15}N H117A GlbN sample (100 mM phosphate, pH 7.1, 10 % D_2O, 298 K, GODCAT) obtained ~2 h after addition of 8 mM DT in the presence of 4 mM ^{15}N-nitrite. ^{15}N decoupling (centered at 117 ppm) was applied during ^{1}H detection. A ^{1}H doublet at ~14.9 ppm, attributed to H^{15}NO bound to Fe^{II} H117A GlbN, was detected with ~ 36% intensity of that of the backbone amide ^{1}H signals of Thr80. (B) Expansion of (A). The ~14.9 ppm $\underline{H}^{15}$NO signal was split by $|^{1}J_{NH}|$ = 71 Hz. ^{15}N decoupling centered at 550 ppm collapsed the splitting (not shown). (C) Decoupled ^{1}H-^{15}N HSQC spectrum of Fe^{II}–H^{15}NO H117A GlbN.

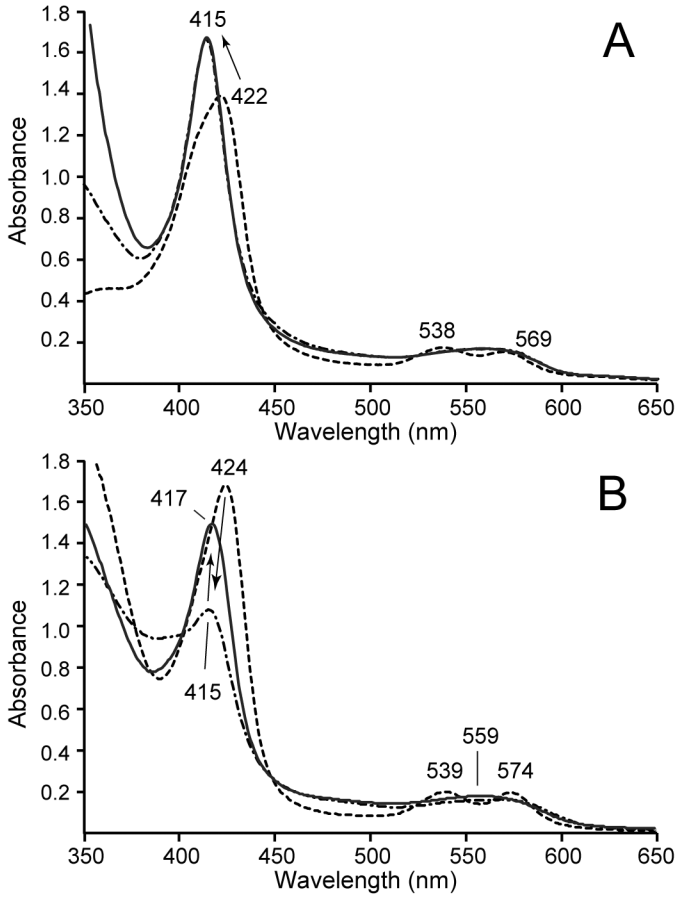

Fig. 8.

Reduction of Fe^{III}–NO GlbN-A and GlbN using heme-free diaphorase and NADPH. (A) The Fe^{III}–NO GlbN-A species (dashed trace) was generated by treatment of Fe^{III} *bis*–histidine GlbN-A with excess MAHMA-NONOate. Some residual Fe^{III} *bis*–histidine species is present. Addition of NADPH and heme-free diaphorase resulted in the formation of Fe^{II}–NO GlbN-A (dash-dot line), with minimal spectral change upon addition of DT (solid trace). (B) The Fe^{III}–NO GlbN species (dashed trace) was slowly converted to Fe^{II}–NO GlbN (dash-dot trace) by incubation with the heme-free diaphorase and NADPH for 70 min. Addition of DT then resulted in the gradual formation of Fe^{II}–HNO GlbN (solid trace, ~4 h after DT addition) as evidenced by the increase of the Soret peak to 417 nm.

Table 1.

Absorption maxima of various forms of GlbN

Ligation state	GlbN γ, β, α (nm)	GlbN-A γ, β, α (nm)
His–Fe^{III}–His	411, ~544	408, ~544
His–Fe^{II}–O_2	411, 550, 584	408, 550, ~585
His–Fe^{III}–NO	424, 538, 574	424, 538, 571
His–Fe^{II}–His	–	425, 527, 558
His–Fe^{II}–NO[a]	~416, ~563	~415, 560
His–Fe^{II}–HNO[a]	~417, ~559	–

[a]Approximate value because of the presence of other species

Table 2.

Heme and HNO proton chemical shifts (pH 7.1, 298 K)

	Fe^{III}–NO GlbN-A	Fe^{III}–NO GlbN	Fe^{II}–HNO GlbN
1-CH_3	3.44	3.40	3.39
2-α	6.81	7.96	7.90
2-$\beta_{cis,trans}$	–	6.16, 6.04	5.75, 5.85
2-β-CH_3	2.36	–	–
α-meso	9.75	9.80	9.28
3-CH_3	3.56	3.53	3.32
4-α	7.80	7.71	7.55
4-$\beta_{cis,trans}$	5.94, 6.30	5.95, 6.12	5.61, 5.88
β-meso	9.52	9.36	8.83
5-CH_3	2.97	3.03	2.68
γ-meso	10.32	10.30	9.63
8-CH_3	3.35	3.33	3.15
δ-meso	9.97	9.96	9.41
HNO	–	–	14.82 14.91 (H117A)